

Joint Structural Break Detection and Parameter Estimation in High-Dimensional Non-Stationary VAR models

Abolfazl Safikhani* and Ali Shojaie†

Columbia University and University of Washington

May 18, 2022

Abstract

Assuming stationarity is unrealistic in many time series applications. A more realistic alternative is to allow for piecewise stationarity, where the model is allowed to change at given time points. We propose a three-stage procedure for consistent estimation of both structural change points and parameters of high-dimensional piecewise vector autoregressive (VAR) models. In the first step, we reformulate the change point detection problem as a high-dimensional variable selection one, and propose a penalized least square estimator using a total variation penalty. We show that the proposed penalized estimation method overestimates the number of change points. We then propose a backward selection criterion in conjunction with a penalized least square estimator to tackle this issue. In the last step of our procedure, we estimate the VAR parameters in each of the segments. We prove that the proposed procedure consistently detects the number of change points and their locations. We also show that the procedure consistently estimates the VAR parameters. The performance of the method is illustrated through several simulation scenarios and real data examples.

Keywords: High-dimensional time series; Piecewise stationarity; Structural breaks; Total variation penalty.

1 Introduction

Emerging applications in biology (Michailidis & dAlché Buc 2013; Smith 2012; Fujita *et al.* 2007; Mukhopadhyay & Chatterjee 2006) and finance (De Mol *et al.* 2008; Fan *et al.* 2011) have sparked an interest in methods for analyzing high-dimensional time series. Recent work includes new regularized estimation procedures for vector autoregressive (VAR) models (Basu & Michailidis 2015; Nicholson *et al.* 2017), high-dimensional generalized linear models (Hall *et al.* 2016) and high-dimensional point processes (Hansen *et al.* 2015; Chen *et al.* 2017). These methods generalize the earlier work on methods for high-dimensional longitudinal data (Shojaie & Michailidis 2010), and handle the theoretical challenges stemming from the temporal dependence among observations. Related methods have also focused on joint estimation of multiple time series (Qiu *et al.* 2016), estimation of (inverse) covariance matrices (Xiao & Wu 2012; Chen *et al.* 2013; Tank *et al.* 2015), and estimation of high-dimensional systems of differential equations (Lu *et al.* 2011; Chen *et al.* 2016).

Despite considerable progress in computational and theoretical fronts, the vast majority of existing work on high-dimensional time series assumes that the underlying process is *stationary*. However, multivariate time series observed in many modern applications are nonstationary. For instance, Clarida *et al.* (2000) show that the effect of inflation on interest rates varies across Federal Reserve regimes. Similarly, as pointed out by Ombao *et al.* (2005), electroencephalograms (EEGs) recorded during an epileptic seizure display amplitudes

*as5012@columbia.edu

†ashojaie@uw.edu

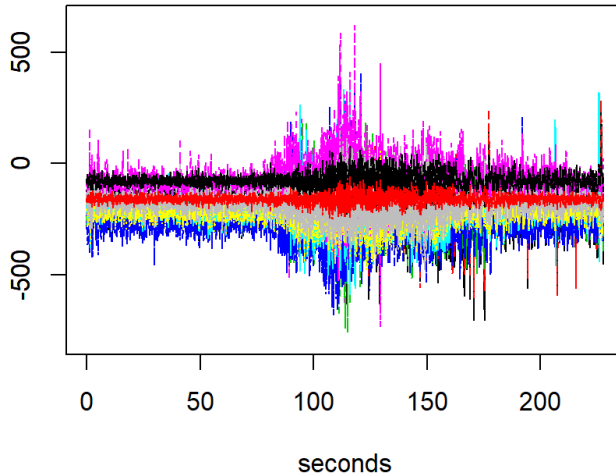


Figure 1: EEG signals from a patient diagnosed with left temporal lobe epilepsy. The data was recorded at 18 locations on the scalp during an epileptic seizure over 22,768 time points.

and spectral distribution that vary over time. This nonstationarity is illustrated in Figure 1, which shows the EEG signals recorded at 18 EEG channels during an epileptic seizure from a patient diagnosed with left temporal lobe epilepsy (Ombao *et al.* 2005). The sampling rate in this data is 100 Hz and the total number of time points per EEG is $T = 22,768$ over ~ 228 seconds. Based on the neurologist’s estimate, the seizure took place at $t = 85$ s. The EEG plot in Figure 1 also suggests that the magnitude and the variability of these signals change simultaneously around that time.

Detecting structural break points in high-dimensional time series and obtaining reliable estimates of model parameters are important from multiple perspectives. First, structural breaks often reveal important changes in the underlying system and are of scientific importance. In our EEG example, automatic detection of structural breaks can assist clinicians in identifying seizures. Second, changes in model parameters before and after break points often provide important scientific insight. For instance, the occurrence of epileptic seizure is expected to change mechanisms of interactions among brain regions. Such changes can be seen in Figure 2. The figure shows networks of interactions among EEG channels before and after seizure. These networks are obtained from estimates using our proposed method, following the procedure described in Section 7. Briefly, edges in the first two networks correspond to *Granger causal* relations (Granger 1969) among EEG channels before and after the period of seizure; the occurrence of seizure is also automatically detected using the proposed method. It can be seen that while the two networks share many edges, they also exhibit important differences. Perhaps most notable are changes in connectivity patterns of channels T5, P3 and Pz, which measure brain activity in the left temporal lobe, which is the cite of epilepsy in the patient. Without reliable estimates of model parameters, gaining such scientific insight may not be feasible. Finally, identifying structural breaks in time series is also crucial for proper analysis of the data. The last network in Figure 2 shows the network of interactions obtained from the full EEG data, ignoring the structural break due to seizure. This network is much more dense than the other two, and is in fact close to a fully connected network, which is rather unexpected. This example underscores that ignoring the structural breaks and assuming stationarity when analyzing times series can severely bias estimation and inference procedures.

In this paper we develop a regularized estimation procedure for simultaneous detection of break points and estimation of model parameters in high-dimensional piecewise stationary VARs with possibly many break points. The proposed approach first identifies the number of break points. It then determines the location of the break points and provides consistent estimates of model parameters.

The rest of this paper is organized as follows. Before describing the piecewise stationary model in Section 2, we review some of the related procedures for nonstationary time series in Section 1.1. An initial

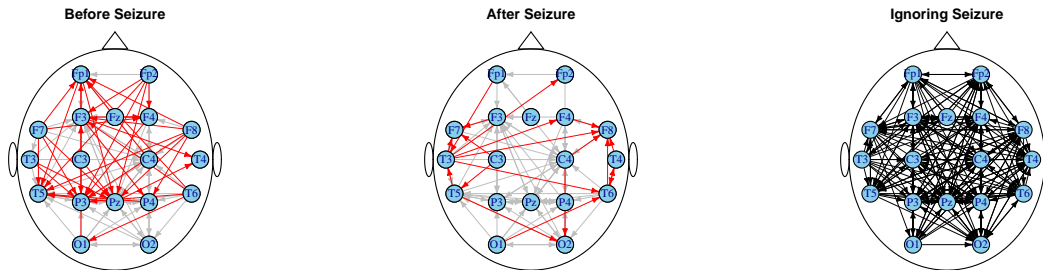


Figure 2: Network of Granger causal interactions among EEG channels based on data from Figure 1. The plots show the schematic locations of the EEG channels. The first two figures show interactions among EEG channels before and after the period of seizure. Gray edges in these two networks show common edges, while red edges show interactions identified either before or after seizure. The network on the right shows interactions from an estimate obtained by ignoring the structural break in the time series.

estimation procedure together with its asymptotic properties are discussed in Section 3. In Section 4, we show that under reasonable assumptions, the structural breaks in high-dimensional VAR models are consistently estimated. Our procedure for consistent parameter estimation is presented in Section 5. Results of simulation experiments are presented in Section 6. In Section 7, we illustrate the utility of the proposed method by applying it to identify structural break points in two multivariate time series. We conclude the paper with a discussion in Section 8. Technical lemmas and proofs are collected in the Appendix.

1.1 Related Methods for Nonstationary Time Series

Non-stationary VAR models have been primarily studied in univariate or low-dimensional settings. Existing approaches include models that fully parameterize the evolution of the transition matrices of time-varying VARs, or enforce a Bayesian prior on the structure of the time-dependence (Primiceri 2005). An alternative approach is to assume that the VAR process is *locally stationary*; locally stationarity means that, in each small time interval, the process is well-approximated by a stationary one. This notion has been studied in low-dimensions by Dahlhaus (2012); Sato *et al.* (2007) proposed a wavelet-based method for estimating the time-varying coefficients of the VAR model.

Recently, Ding *et al.* (2016) considered estimation of high-dimensional time-varying VARs by solving time-varying Yule-Walker equations based on kernelized estimates of variance and auto-covariance matrices. This approach facilitates estimation of locally stationary VAR models in high dimensions. However, local stationarity may not be a suitable assumption in many applications. For instance, in the EEG example of Section 1, assuming that the process can be locally approximated by a stationary one at the time of seizure may be unrealistic. A more natural assumption in such settings is that the process is *piecewise stationary* — i.e., the process is stationary in each of (potentially many) regions, e.g., before and after seizure.

A number of methods have been proposed for analyzing univariate piecewise stationary time series. For instance, Davis *et al.* (2006), Chan *et al.* (2014) and Bai (1997) propose different approaches for identifying structural breakpoints at which the behavior of a univariate time series changes. The problem of change point detection in multivariate time series has also been considered in few recent publications. In particular, the SLEX method of Ombao *et al.* (2005) uses time-varying wavelets to detect changes in multivariate time series, and the proposed test procedure in Aue *et al.* (2009) can identify breaks in the covariance structure of multivariate, and possibly non-linear, time series. More recently, Cho & Fryzlewicz (2015) used sparsified binary segmentation to detect structural break points in multivariate time series, whereas Cho *et al.* (2016) utilized a double CUSUM statistic to detect (multiple) break points in multivariate time series models. However, existing multivariate approaches do not provide estimates of model parameters: To deal with the large number of time series, Ombao *et al.* (2005) apply a dimension reduction step, whereas Cho & Fryzlewicz (2015) use a CUSUM statistic. As a result, both methods only estimate the structural break points. In other words, while these methods can indeed identify the structural breaks in the EEG example, they do not reveal mechanisms of interactions among brain regions, which is of key interest for understanding changes in brain

function before and after seizure. As discussed in Section 5, consistent estimation of model parameters in high-dimensional piecewise stationary VAR models introduces new challenges. Addressing these challenges and providing interpretable estimates of parameters in high-dimensional piecewise stationary VAR models are two key contributions of the current paper.

2 Piecewise Stationary VAR Models

A piecewise stationary VAR model can be viewed as a collection of separate VAR models concatenated at multiple break points over the observed time period. More specifically, suppose there exist m_0 break points $0 = t_0 < t_1 < \dots < t_{m_0} < t_{m_0+1} = T + 1$ such that for $t_{j-1} \leq t < t_j, j = 1, \dots, m_0 + 1$,

$$y_t = \Phi^{(1,j)} y_{t-1} + \dots + \Phi^{(q,j)} y_{t-q} + \Sigma_j^{1/2} \varepsilon_t. \quad (1)$$

Here, y_t is the p -vector of observed time series at time t ; $\Phi^{(l,j)} \in \mathbb{R}^{p \times p}$ is the (sparse) coefficient matrix corresponding to the l th lag of a VAR process of order q during for the j th segment $j = 1, \dots, m_0 + 1$; ε_t is a multivariate Gaussian white noise with independent components, and Σ_j is the covariance matrix of the noise for the j th segment. To simplify the notations, we henceforth denote the noise as ε_t without specifying the covariance Σ_j , but allow for noise terms to have different covariance matrices in different segments.

Our goal is to detect the break points, t_j , together with estimates of the coefficient parameters $\Phi^{(l,j)}$ in the high-dimensional case where $p \gg T$. To this end, we generalize the change-point detection ideas of Harchaoui & Lévy-Leduc (2010) and Chan *et al.* (2014) to the multivariate, high-dimensional setting, and extend it to obtain consistent estimates of model parameters. More specifically, our estimation procedure utilizes the following linear regression representation of the VAR process

$$\begin{pmatrix} y'_q \\ y'_{q+1} \\ \vdots \\ y'_T \end{pmatrix} = \begin{pmatrix} y'_{q-1} & \dots & y'_0 & 0 & \dots & 0 \\ y'_q & \dots & y'_1 & y'_q & \dots & y'_1 & \dots & 0 \\ \vdots & \vdots & \vdots & \vdots & \ddots & \vdots & \vdots & \vdots \\ y'_{T-1} & \dots & y'_{T-q} & y'_{T-1} & \dots & y'_{T-q} & \dots & y'_{T-1} & \dots & y'_{T-q} \end{pmatrix} \begin{pmatrix} \theta'_1 \\ \theta'_2 \\ \vdots \\ \theta'_n \end{pmatrix} + \begin{pmatrix} \varepsilon'_q \\ \varepsilon'_{q+1} \\ \vdots \\ \varepsilon'_T \end{pmatrix}, \quad (2)$$

where $n = T - q + 1$, $\Phi^{(\cdot,j)} = (\Phi^{(1,j)} \dots \Phi^{(q,j)}) \in \mathbb{R}^{p \times pq}$, $\theta_1 = \Phi^{(\cdot,1)}$ and for $i = 2, 3, \dots, n$,

$$\theta_i = \begin{cases} \Phi^{(\cdot,i+1)} - \Phi^{(\cdot,i)}, & \text{when } i = t_j \text{ for some } j \\ 0, & \text{otherwise.} \end{cases} \quad (3)$$

Throughout the paper, the transpose of a matrix A is denoted by A' . Note that in this parameterization, $\theta_i \neq 0$ for $i \geq 2$ implies a change in the VAR coefficients. Therefore, the structural break points $t_j, j = 1, \dots, m_0$ can be estimated as time points $i \geq 2$, where $\theta_i \neq 0$.

Equation 2 is a linear regression of the form

$$\mathcal{Y} = \mathcal{X}\Theta + E$$

which can be written in vector form as

$$\mathbf{Y} = \mathbf{Z}\Theta + \mathbf{E}, \quad (4)$$

where $\mathbf{Y} = \text{vec}(\mathcal{Y})$, $\mathbf{Z} = I_p \otimes \mathcal{X}$, and $\mathbf{E} = \text{vec}(E)$. Denoting $\pi = np^2q$, $\mathbf{Y} \in \mathbb{R}^{np \times 1}$, $\mathbf{Z} \in \mathbb{R}^{np \times \pi}$, $\Theta \in \mathbb{R}^{\pi \times 1}$, and $\mathbf{E} \in \mathbb{R}^{np \times 1}$.

3 An Initial Estimator

The linear regression representation in (4) suggests that the model parameters Θ can be estimated via regularized least squares. The regularization is necessary to both handle the growing number of parameters corresponding to potential change points, as well as the number of time series p . A simple initial estimate of parameters Θ can thus be obtained by using an ℓ_1 penalized least squares regression of the form

$$\hat{\Theta} = \underset{\Theta}{\text{argmin}} \frac{1}{n} \|\mathbf{Y} - \mathbf{Z}\Theta\|_2^2 + \lambda_n \|\Theta\|_1. \quad (5)$$

The optimization problem in (5) is convex and can be efficiently solved using a block coordinate descent algorithm (Tseng & Yun 2009). This algorithm involves updating one of the θ_i 's at each iteration, until convergence. The KKT conditions of problem (5), presented in Lemma 2 of Appendix A, show that for fixed $i = 1, 2, \dots, n$, the θ_i update at iteration $h + 1$ can be obtained in closed form as

$$\theta_i^{(h+1)} = \left(\sum_{l=i}^n Y_{l-1} Y'_{l-1} \right)^{-1} S \left(\sum_{l=i}^n Y_{l-1} y_l - \sum_{j \neq i} \left(\sum_{l=\max(i,j)}^n Y_{l-1} Y'_{l-1} \right) \theta_j^{(h)}; \lambda \right), \quad (6)$$

where $Y'_l = (y'_l \dots y'_{l-q+1})_{1 \times pq}$. Here, $S(\cdot; \lambda)$ is the element-wise soft-thresholding function on all the components of the input matrix, which maps its input x to $x - \lambda$ when $x > \lambda$, $x + \lambda$ when $x < -\lambda$, and 0 when $|x| \leq \lambda$. The iteration stops when $\|\theta^{(h+1)} - \theta^{(h)}\|_\infty < \delta$, where δ is the tolerance set to 10^{-3} in our implementation. Here and throughout the paper, for a $m \times n$ matrix A , $\|A\|_\infty = \max_{1 \leq i \leq m, 1 \leq j \leq n} |a_{ij}|$. Note that in this algorithm, the whole block of θ_i with p^2q elements is updated at once, which reduces the computation time dramatically.

Despite its convenience and computational efficiency, estimates from (5) do not correctly identify the structural break points in the piecewise VAR process. In fact, our theoretical analysis in the next part shows that the number of estimated break points from (5), i.e., the number of nonzero $\hat{\theta}_i \neq 0$, $i \geq 2$, over-estimates the true number of break points. This is because the design matrix \mathbf{Z} may not satisfy the restricted eigenvalue condition (Bickel *et al.* 2009) necessary for establishing consistent estimation of parameters. However, as we show in Section 3.1, the model from (5) does achieve prediction consistency. In Section 4 we show that this initial estimator can be refined in order to obtain consistent estimates of structural break points.

3.1 Asymptotic Properties

Denote the set of estimated change points from (5) by

$$\mathcal{A}_n = \left\{ i \geq 2 : \hat{\theta}_i \neq 0 \right\}.$$

The total number of estimated change points is then the cardinality of the set \mathcal{A}_n ; denote $\hat{m} = |\mathcal{A}_n|$. Let $\hat{t}_j, j = 1, \dots, \hat{m}$ be the estimated break points. Then, the relationship between $\hat{\theta}_j$ and $\hat{\Phi}^{(\cdot, j)}$ in each of the estimated segments can be seen as:

$$\hat{\Phi}^{(\cdot, 1)} = \hat{\theta}_1, \quad \text{and} \quad \hat{\Phi}^{(\cdot, j)} = \sum_{i=1}^{\hat{t}_j} \hat{\theta}_i, \quad j = 1, 2, \dots, \hat{m}. \quad (7)$$

In this section, we show that $\hat{m} \geq m_0$. We also show that there exist m_0 points within \mathcal{A}_n that are ‘close’ to the true break points. To this end, we first establish that if the number of change points m_0 is known, the estimator (5) can consistently recover the break points. Using a more careful analysis, we then show that in the case when m_0 is unknown, the penalized least squares (5) identifies a larger set of *candidate* break points. These result justify the second step of our estimation procedure described in the Section 4, which searches over the break points in \mathcal{A}_n in order to identify an optimal set of break points. In fact, in Section 4 we show that using an information criterion combining (a) regular least squares, (b) the ℓ_1 norm of the estimated parameters, and (c) a term penalizing the number of break points, we are able to complete the search and correctly identify the number of segments in the model.

To establish the asymptotic properties of our initial estimator, we make the following assumptions. We first define a few notations.

Denote the number of nonzero elements in the k -th row of $\Phi^{(\cdot, j)}$ by d_{kj} , $k = 1, 2, \dots, p$ and $j = 1, 2, \dots, m_0$. Further, for each $j = 1, 2, \dots, m_0 + 1$ and $k = 1, \dots, p$, define \mathcal{I}_{kj} to be the set of all column indexes of $\Phi_k^{(\cdot, j)}$ at which there is a nonzero term, where $\Phi_k^{(\cdot, j)}$ denotes the k -th row of $\Phi^{(\cdot, j)}$. Let $\mathcal{I} = \cup_{k,j} \mathcal{I}_{kj}$, and define $d_n = \max_{1 \leq k \leq p, 1 \leq j \leq m_0+1} |\mathcal{I}_{kj}|$.

A1 For each fixed $j = 1, 2, \dots, m_0 + 1$, the process $y_t^{(j)} = \Phi^{(1,j)} y_{t-1}^{(j)} + \dots + \Phi^{(q,j)} y_{t-q}^{(j)} + \Sigma_j^{1/2} \varepsilon_t$ is a stationary Gaussian time series. Denote the covariance matrices $\Gamma_j(h) = \text{cov} \left(y_t^{(j)}, y_{t+h}^{(j)} \right)$ for $t, h \in \mathbb{Z}$.

Also, assume that for $\kappa \in [-\pi, \pi]$, the spectral density matrices $f_j(\kappa) = (2\pi)^{-1} \sum_{l \in \mathbb{Z}} \Gamma_j(l) e^{-il\kappa}$ exist; further

$$\max_{1 \leq j \leq m_0+1} \mathcal{M}(f_j) = \max_{1 \leq j \leq m_0+1} \left(\text{ess sup}_{\kappa \in [-\pi, \pi]} \Lambda_{\max}(f_j(\kappa)) \right) < +\infty,$$

and

$$\min_{1 \leq j \leq m_0+1} \mathbf{m}(f_j) = \min_{1 \leq j \leq m_0+1} \left(\text{ess sup}_{\kappa \in [-\pi, \pi]} \Lambda_{\min}(f_j(\kappa)) \right) > 0,$$

where $\Lambda_{\max}(A)$ and $\Lambda_{\min}(A)$ are the largest and smallest eigenvalue of the symmetric or Hermitian matrix A , respectively.

A2 The matrices $\Phi^{(\cdot, j)}$ are sparse. More specifically, $d_{kj} \ll p$ for all $k = 1, 2, \dots, p$ and $j = 1, 2, \dots, m_0$. Moreover, there exists a positive constant $M_\Phi > 0$ such that,

$$\max_{1 \leq j \leq m_0+1} \left\| \Phi^{(\cdot, j)} \right\|_\infty \leq M_\Phi.$$

A3 There exists a positive constant v such that,

$$\min_{1 \leq j \leq m_0} \max_{1 \leq k \leq p} \left\| \Phi_k^{(\cdot, j+1)} \right\|_2 - \left\| \Phi_k^{(\cdot, j)} \right\|_2 \geq v > 0.$$

Moreover, there exists a vanishing positive sequence γ_n such that as $n \rightarrow \infty$,

$$\min_{1 \leq j \leq m_0+1} |t_j - t_{j-1}| / (n\gamma_n) \rightarrow +\infty, \quad \gamma_n / (d_n \lambda_n) \rightarrow +\infty, \quad \log(p) / (n\gamma_n) \rightarrow 0 \quad \text{and} \quad d_n \sqrt{\frac{\log p}{n\gamma_n}} \rightarrow 0.$$

Assumption A1 is needed to achieve appropriate probability bounds in high dimensions. This assumption does not restrict the applicability of the method since it is valid for large families of VAR models (Basu & Michailidis 2015). The second part of A1 will also be needed in the proof of consistency of the VAR parameters once the break points are detected. Assumption A2 is related to the total sparsity of the model. The sequence γ_n is directly related to the detection rate of the break points $t_j, j = 1, \dots, m_0$. Assumption A3 connects this rate to the tuning parameter chosen in the estimation procedure. Also, this assumption puts a minimum distance-type requirement on the coefficients in different segments. This can be regarded as the extension of assumption H2 in Chan *et al.* (2014) from univariate to the high-dimensional case.

As pointed out earlier, and discussed in Chan *et al.* (2014) and Harchaoui & Lévy-Leduc (2010), the design matrix \mathbf{Z} in (4) may not satisfy the restricted eigenvalue condition needed for parameter estimation consistency (Bickel *et al.* 2009). Thus, as a first step towards establishing the consistency of the proposed procedure, in this section we establish the prediction consistency of the estimator from (5).

Theorem 1. *Suppose A1 and A2 hold. Choose $\lambda_n = 2C \sqrt{\frac{\log(n)+2 \log(p)+\log(q)}{n}}$ for some $C > 0$. Also, assume $m_0 \leq m_n$ with $m_n = o(\lambda_n^{-1})$. Then, with high probability approaching 1 as $n \rightarrow +\infty$,*

$$\frac{1}{n} \left\| \mathbf{Z} \left(\widehat{\Theta} - \Theta \right) \right\|_2^2 \leq 2M_\Phi \lambda_n m_n \max_{1 \leq j \leq m_0+1} \left\{ \sum_{k=1}^p (d_{kj} + d_{k(j-1)}) \right\}. \quad (8)$$

Theorem 1 is proved in Appendix B. Note that this theorem imposes an upper bound on the model sparsity, as the right hand side of (8) must go to zero as $n \rightarrow \infty$. In Section 4, we specify the limit on the sparsity needed for consistent identification of structural break points.

Next, we study a simplified version of the problem, by assuming that the true number of change points are known and used in the estimation. In this case, the task reduces to locating the break points. We obtain the following result for this simplified problem.

Theorem 2. *Suppose A1–A3 hold. If m_0 is known and $|\mathcal{A}_n| = m_0$, then*

$$\mathbb{P} \left(\max_{1 \leq j \leq m_0} |\widehat{t}_j - t_j| \leq n\gamma_n \right) \rightarrow 1, \quad \text{as } n \rightarrow +\infty.$$

Theorem 2, which is merely an intermediate result, is proved in Appendix B. The proof relies on the KKT condition for the problem (5), stated in Lemma 2 and the probability bounds in Lemma 3; these lemmas are given in the Appendix A.

The rate of consistency for break point detection in Theorem 2 is $n\gamma_n$, which can be chosen as small as possible assuming that Assumptions A2 and A3 hold. γ_n also depends on the minimum distance between consecutive true break points, as well as the number of time series, p . When m_0 is finite, one can choose $\gamma_n = (\log n \log p)/n$ or $\gamma_n = (\log \log n \log p)/n$. This means that the convergence rate for estimating the relative locations of the break points, i.e., t_j/T using \hat{t}_j/T , could be as low as $(\log \log n \log p)/n$. In the univariate case, Chan *et al.* (2014) showed a convergence of order $(\log n)/n$. The rate found here is larger than the univariate case by an order less than $\log p$ — this logarithmic factor captures the additional difficulty in estimating the structural break points in high-dimensional settings.

We now turn to the more general case of unknown m_0 . Our next result shows that the number of selected change points, \hat{m} , based on the estimation procedure (5) will be at least as large as the true number m_0 . Moreover, each true change point will have at least one estimated point in its $n\gamma_n$ -radius neighborhood.

Before stating the theorem, we need some additional notations. Let $\mathcal{A} = \{t_1, t_2, \dots, t_{m_0}\}$ be the set of true change points. Following Boysen *et al.* (2009) and Chan *et al.* (2014), define the Hausdorff distance between two sets as

$$d_H(A, B) = \max_{b \in B} \min_{a \in A} |b - a|.$$

We obtain the following results.

Theorem 3. *Suppose A1–A3 hold. Then as $n \rightarrow +\infty$,*

$$\mathbb{P}(|\mathcal{A}_n| \geq m_0) \rightarrow 1,$$

and

$$\mathbb{P}(d_H(\mathcal{A}_n, \mathcal{A}) \leq n\gamma_n) \rightarrow 1.$$

The second part of Theorem 3 shows that even though we select more points than needed, there exists a subset of the estimated points of size m_0 , which estimates the true break points at the same rate as if m_0 was known. This result motivates the second stage of our estimation procedure, discussed in the next section, which removes the additional estimated break points.

4 Consistent Estimation of Structural Breaks

Theorem 3 shows that the penalized estimation procedure (5) over-estimates the number of change points. A second stage screening is thus needed to screen out the additional estimated change points and consistently estimate the true change points. To this end, we propose next a screening procedure, which is a modification of the procedure in Chan *et al.* (2014). The basic idea is to develop an *information criterion* based on a new penalized least squares estimation procedure, in order to screen the candidate break points found in the first estimation stage. Formally, for a fixed m and estimated change points s_1, \dots, s_m , we form the following linear regression:

$$\begin{pmatrix} y'_q \\ y'_{q+1} \\ \vdots \\ y'_T \end{pmatrix} = \begin{pmatrix} Y'_{q-1} & & & \\ \vdots & 0 & \dots & 0 \\ Y'_{s_1-1} & & & \\ & Y'_{s_1} & & \\ 0 & \vdots & \dots & 0 \\ & Y'_{s_2-1} & & \\ \vdots & \vdots & \ddots & \vdots \\ & & & Y'_{s_m} \\ 0 & 0 & & \vdots \\ & & & Y'_T \end{pmatrix} \begin{pmatrix} \theta'_1 \\ \theta'_2 \\ \vdots \\ \theta'_{m+1} \end{pmatrix} + \begin{pmatrix} \xi'_q \\ \xi'_{q+1} \\ \vdots \\ \xi'_T \end{pmatrix}. \quad (9)$$

As in Section 2, this regression can be written compactly as

$$\mathcal{Y} = \mathcal{X}_{s_1, \dots, s_m} \theta_{s_1, \dots, s_m} + \Xi,$$

where $\mathcal{X}_{s_1, \dots, s_m} \in \mathbb{R}^{n \times \pi_m}$, $\theta_{s_1, \dots, s_m} = \left(\theta'_{(1, s_1)}, \theta'_{(s_1, s_2)}, \dots, \theta'_{(s_m, T)} \right)' \in \mathbb{R}^{\pi_m \times p}$, with $\pi_m = (m+1)pq$. We estimate θ_{s_1, \dots, s_m} using the following penalized regression:

$$\hat{\theta}_{s_1, \dots, s_m} = \operatorname{argmin}_{\theta} \sum_{i=1}^{m+1} \left(\frac{1}{s_i - s_{i-1}} \sum_{t=s_{i-1}}^{s_i-1} \|y_t - \theta_i Y_{t-1}\|_2^2 + \eta_{(s_{i-1}, s_i)} \|\theta_i\|_1 \right), \quad (10)$$

with tuning parameters $\eta_n = (\eta_{(s_0, s_1)}, \dots, \eta_{(s_m, s_{m+1})})$, where $s_0 = q$ and $s_{m+1} = T$.

Define

$$L_n(s_1, s_2, \dots, s_m; \eta_n) = \|\mathcal{Y} - \mathcal{X}_{s_1, \dots, s_m} \hat{\theta}_{s_1, \dots, s_m}\|_F^2 + \sum_{i=1}^{m+1} \eta_{(s_{i-1}, s_i)} \|\hat{\theta}_{(s_{i-1}, s_i)}\|_1. \quad (11)$$

Then, for a suitably chosen sequence ω_n , specified in Assumption A4 below, consider the following information criterion:

$$\operatorname{IC}(s_1, \dots, s_m; \eta_n) = L_n(s_1, s_2, \dots, s_m; \eta_n) + m\omega_n.$$

The second stage of our procedure selects a subset of \hat{m} break points by solving the problem

$$(\tilde{m}, \tilde{t}_j, j = 1, \dots, \tilde{m}) = \operatorname{argmin}_{0 \leq m \leq \hat{m}, \mathbf{s}=(s_1, \dots, s_m) \in \mathcal{A}_n} \operatorname{IC}(\mathbf{s}; \eta_n). \quad (12)$$

To establish the consistency of the proposed screening procedure (12), we need two additional assumptions. In the following, $d_n^* = \sum_{j=1}^{m_0+1} \sum_{k=1}^p d_{kj}$ is the total sparsity of the model.

A4 Define $\Delta_n = \min_{1 \leq j \leq m_0} |t_{j+1} - t_j|$. Then, $m_0 n \gamma_n d_n^{*2} / \omega_n \rightarrow 0$, and $\Delta_n / (m_0 \omega_n) \rightarrow +\infty$.

A5 There exist a large positive constant $c > 0$ such that (a) if $|s_i - s_{i-1}| \leq n\gamma_n$, then $\eta_{(s_{i-1}, s_i)} = c\sqrt{n\gamma_n \log p}$; (b) if there exist t_j, t_{j+1} such that $|s_{i-1} - t_j| \leq n\gamma_n$ and $|s_i - t_{j+1}| \leq n\gamma_n$, then, $\eta_{(s_{i-1}, s_i)} = 2 \left(c\sqrt{\frac{\log p}{s_i - s_{i-1}}} + M_{\Phi} d_n^* \frac{n\gamma_n}{s_i - s_{i-1}} \right)$; (c) otherwise, $\eta_{(s_{i-1}, s_i)} = 2 \left(c\sqrt{\frac{\log p}{s_i - s_{i-1}}} + M_{\Phi} d_n^* \right)$.

We can now state our main consistency result.

Theorem 4. *Suppose A1–A5 hold. Then, as $n \rightarrow +\infty$, the minimizer $(\tilde{m}, \tilde{t}_j, j = 1, \dots, \tilde{m})$ of (12) satisfies*

$$\mathbb{P}(\tilde{m} = m_0) \rightarrow 1.$$

Moreover, there exists a positive constant $B > 0$ such that

$$\mathbb{P} \left(\max_{1 \leq j \leq m_0} |\tilde{t}_j - t_j| \leq B m_0 n \gamma_n d_n^{*2} \right) \rightarrow 1.$$

The proof of the theorem, given in Appendix B relies heavily on the result presented in Lemma 4, which is stated and derived in Appendix A.

Remark 1. For the case when m_0 is finite, the rates can be set to $\gamma_n = (\log n \log p)/n$, $\lambda_n = o((\log n \log p)/np)$, and $\omega_n = (\log n \log p)^{1+\nu}$ for some positive $\nu > 0$. For these rates, the model can have total sparsity $d_n^* = o((\log n \log p)^{\nu/2})$.

Remark 2. The proposed three-stage procedure can be also applied to low-dimensional time series. For example, with $p = cn^a$ for positive constants c, a , the probability bounds derived in Lemma 3 would be strong enough to obtain the desired consistency results shown for the high-dimensional case.

Remark 3. Selecting the tuning parameter η in Assumption A5 is challenging in practice, since the distance between candidate break points from the initial estimation to the true break points is unknown. Thus, while the specified tuning parameters achieve optimal consistency rates for locating the break points, they are not practical in finite sample settings and application. To overcome this challenge, we can instead consider a fixed tuning parameter η in all the candidate segments as $\eta = C m_0 \sqrt{\Delta_n^* \log p}/n$ for some large

enough positive constant $C > 0$, where $\Delta_n^* = \max_{1 \leq j \leq m_0} |t_{j+1} - t_j|$. We can still show the consistency of the proposed procedure in (12) with this fixed η . However, the consistency rate for locating the break points using this fixed rate would be different from that achieved in Theorem 4. For finite m_0 , the rate would be of order $(n \log p)^{1/2+\nu}$ for some positive $\nu > 0$ as compared to the rate $(\log n \log p)^{1+\nu}$ when the tuning parameters are selected as in Assumption A5. In all simulation studies and real data applications, η was selected according to the fixed rate mentioned in this remark.

When the number of change points selected at the first stage $|\mathcal{A}_n|$ is large, the second screening step to find the minimizer of the information criterion IC would be computationally demanding. In order to reduce the computational cost, we here propose a backward elimination algorithm (BEA) to approximate the optimal point at a lower computational cost. The idea of our BEA algorithm, which is similar to that in Chan *et al.* (2014), is to start with the full set of selected points, \mathcal{A}_n , and in each step remove one unnecessary point until no further reduction is possible. More specifically, the algorithm is as follows:

- (i) Set $m = |\mathcal{A}_n|$. Let $\mathbf{s} = \{s_1, \dots, s_m\}$ be the selected points and define $W_m^* = \text{IC}(s_1, \dots, s_m; \eta_n)$.
- (ii) For each $i = 1, \dots, m$, calculate $W_{m,i} = \text{IC}(\mathbf{s} \setminus \{s_i\}; \eta_n)$. Define $W_{m-1}^* = \min_i W_{m,i}$.
- (iii) (a) If $W_{m-1}^* > W_m^*$, then no further reduction is needed. Return \mathcal{A}_n as the estimated change points.
 (b) If $W_{m-1}^* \leq W_m^*$, and $m > 1$, set $j = \text{argmin}_i W_{m,i}$, set $\mathbf{s} = \mathbf{s} \setminus \{s_j\}$ and $m = m - 1$. Go to step (ii).
 (c) If $W_{m-1}^* \leq W_m^*$ and $m = 1$, all selected points are removed. Return the empty set.

While the proposed BEA algorithm is not guaranteed to achieve the minimizer of (12), it only requires to search \widehat{m}^2 sets in order to find the break points. The algorithm thus results in a significant reduction in the computational time when \widehat{m} is large. The BEA algorithm was used in simulation studies of Section 6 and real data examples of Section 7, and seems to perform very well in all cases.

4.1 Comparison With Other Methods

Before discussing the parameter estimation consistency, in this section, we compare our results on the consistency of break points with two related methods.

Chan *et al.* (2014) investigate the problem of structural break detection for univariate AR processes. When m_0 is finite, their rate of consistency for estimating the location of the break points is of order $(\log n)^{1+\nu}$ some positive $\nu > 0$ under the assumption that the distance between two consecutive break points is at least $(\log n)^{1+\nu}$. Our method can be seen as an extension of Chan *et al.*'s procedure to the high-dimensional setting: Our consistency rate of our method is of order $(\log n \log p)^{1+\nu}$ assuming the consecutive break points distances to be at least of the same order. The additional logarithmic factor $(\log p)^{1+\nu}$ quantifies the complexity of the problem in the high-dimensional case.

The recent proposal of Cho & Fryzlewicz (2015) uses a CUSUM statistic to identify the number of break points together with their locations. The proposal of Cho & Fryzlewicz (2015) is the closest competitor to our approach as it also identifies structural breaks in high-dimensional time series. However, aside from consistent estimation of model parameters discussed in the Introduction, the two methods have a number of differences. First, in Cho & Fryzlewicz (2015), the number of time series p is allowed to grow polynomially with the number of time points T . Our method allows p to grow exponentially with T . Second, the minimum distance between two consecutive break points allowed in (Cho & Fryzlewicz 2015) is of order T^ψ for some $\psi \in (6/7, 1)$. In our setting, depending on the sparsity of the model, this rate could be as low as $\Delta_n = (\log n \log p)^{1+\nu}$ for some positive $\nu > 0$. Therefore, for sparse enough VARs, our method can detect considerably closer break points. Finally, the rate of consistency of our method for estimating the location of the break points is of order $m_0 n \gamma_n d_n^{*2}$, which could be as low as $(\log n \log p)^{1+\nu}$. Cho & Fryzlewicz (2015) can achieve a similar rate when Δ_n is order T . However, when Δ_n is smaller and is of order T^ψ for some $\psi \in (6/7, 1)$, Cho & Fryzlewicz's rate of consistency will be of order $T^{2-2\psi}$, which is considerably larger than our logarithmic rate.

5 Consistent Parameter Estimation

Our results from the previous sections, and in particular, Theorems 4, suggest that we can consistently estimate the location and number of change points in high-dimensional time series. However, even with such estimates, consistent estimation of $\Phi^{(\cdot, j)}$ parameters in nonstationary high-dimensional VAR models remains challenging. This challenge primarily stems from the inexact nature of structural break estimation. More specifically, while we know that the estimated break points are in some neighborhood of the true break points, they are not guaranteed to segment the time series into stationary components. A more careful analysis is thus needed to ensure the consistency of VAR parameters.

The key to our idea for consistent parameter estimation is that Theorems 2 and 4 imply that removing the selected break points together with large enough R_n -radius neighborhoods will also remove the true break points. We can thus obtain stationary segments at the cost of discarding some portions of the time series. When m_0 is known, the radius R_n can be as small as $n\gamma_n$. However, when m_0 is unknown, R_n needs to be at least $Bm_0n\gamma_n d_n^{*2}$ for a large value $B > 0$.

Given the results from Theorems 4, suppose, without loss of generality, that we have selected m_0 break points using the procedure developed in Section 4. Denote these estimated break points by $\tilde{t}_1, \dots, \tilde{t}_{m_0}$. Then, by Theorem 4,

$$\mathbb{P} \left(\max_{1 \leq j \leq m_0} |\tilde{t}_j - t_j| \leq R_n \right) \rightarrow 1,$$

as $n \rightarrow \infty$. Denote $r_{j1} = \tilde{t}_j - R_n - 1$, $r_{j2} = \tilde{t}_j + R_n + 1$ for $j = 1, \dots, m_0$, and set $r_{02} = q$ and $r_{(m_0+1)1} = T$. Further, define the intervals $I_{j+1} = [r_{j2}, r_{(j+1)1}]$ for $j = 0, \dots, m_0$. The idea is to form a linear regression on $\cup_{j=0}^{m_0} I_{j+1}$ and estimate the auto-regressive parameters by minimizing an ℓ_1 -regularized least squares criterion. More specifically, we form the following linear regression:

$$\begin{pmatrix} y'_q \\ \vdots \\ y'_{r_{11}} \\ y'_{r_{12}} \\ \vdots \\ y'_{r_{21}} \\ \vdots \\ y'_{r_{m_01}} \\ \vdots \\ y'_T \end{pmatrix} = \begin{pmatrix} Y'_{q-1} & & & & \\ \vdots & 0 & \dots & 0 & \\ Y'_{r_{11}-1} & & Y'_{r_{12}-1} & & \\ & 0 & \vdots & \dots & 0 \\ & & Y'_{r_{21}-1} & & \\ \vdots & \vdots & \ddots & \vdots & \\ & & & Y'_{r_{m_02}-1} & \\ 0 & 0 & & \vdots & \\ & & & & Y'_{T-1} \end{pmatrix} \begin{pmatrix} \beta'_1 \\ \beta'_2 \\ \vdots \\ \beta'_{m_0+1} \end{pmatrix} + \begin{pmatrix} \zeta'_q \\ \vdots \\ \zeta'_{r_{11}} \\ \zeta'_{r_{12}} \\ \vdots \\ \zeta'_{r_{21}} \\ \vdots \\ \zeta'_{r_{m_01}} \\ \vdots \\ \zeta'_T \end{pmatrix}. \quad (13)$$

This regression can be written in compact form as

$$\mathcal{Y}_{\mathbf{r}} = \mathcal{X}_{\mathbf{r}} \mathbf{B} + \mathbf{E}_{\mathbf{r}}$$

or, in a vector form, as

$$\mathbf{Y}_{\mathbf{r}} = \mathbf{Z}_{\mathbf{r}} \mathbf{B} + \mathbf{E}_{\mathbf{r}} \quad (14)$$

where $\mathbf{Y}_{\mathbf{r}} = \text{vec}(\mathcal{Y}_{\mathbf{r}})$, $\mathbf{Z}_{\mathbf{r}} = I_p \otimes \mathcal{X}_{\mathbf{r}}$, $\mathbf{B} = \text{vec}(\mathbf{B})$, $\mathbf{E}_{\mathbf{r}} = \text{vec}(\mathbf{E}_{\mathbf{r}})$, and \mathbf{r} is the collection of all r_{j1}, r_{j2} for $j = 0, \dots, m_0 + 1$. Denoting $\tilde{\pi} = (m_0 + 1)p^2q$, $N_j = \text{length}(I_{j+1})$ for $j = 0, \dots, m_0$, $N = \sum_{j=1}^{m_0} N_j$, $\mathbf{Y}_{\mathbf{r}} \in \mathbb{R}^{Np \times 1}$, $\mathbf{Z}_{\mathbf{r}} \in \mathbb{R}^{Np \times \tilde{\pi}}$, $\mathbf{B} \in \mathbb{R}^{\tilde{\pi} \times 1}$, and $\mathbf{E}_{\mathbf{r}} \in \mathbb{R}^{Np \times 1}$. Note that $N/n = O(1)$. We estimate the VAR parameters as

$$\hat{\mathbf{B}} = \underset{\mathbf{B}}{\text{argmin}} \frac{1}{N} \|\mathbf{Y}_{\mathbf{r}} - \mathbf{Z}_{\mathbf{r}} \mathbf{B}\|_2^2 + \rho_n \|\mathbf{B}\|_1. \quad (15)$$

We obtain the following consistency result.

Theorem 5. *Suppose A1–A5 hold. Further, suppose either (a) m_0 is known and $R_n = n\gamma_n$; or (b) m_0 is unknown and $R_n = Bm_0n\gamma_nd_n^{*2}$. Assume $\Delta_n > \varepsilon n$ for some large positive $\varepsilon > 0$. Then, for any $\rho_n \geq C\sqrt{\frac{\log \bar{\pi}}{N}}$ for large enough $C > 0$, as $n \rightarrow +\infty$, the minimizer $\hat{\mathbf{B}}$ of (15) satisfies*

$$\left\| \hat{\mathbf{B}} - \Phi \right\|_1 = O_p(d_n^* \rho_n),$$

$$\left\| \hat{\mathbf{B}} - \Phi \right\|_2 = O_p(\sqrt{d_n^*} \rho_n).$$

Theorem 5 is proved in Appendix B.

6 Simulation Studies

In this section, we evaluate the performance of the proposed three-stage estimator with respect to both structural break detection and parameter estimation. We consider three simulation scenarios. In each scenario, 100 data sets are randomly generated with $T = 300$, $p = 20$, $q = 1$ and $m_0 = 2$. All time series have mean zero, and $\Sigma_\varepsilon = 0.01I_T$.

For structural break detection, we compare our estimator with the sparsified binary segmentation-multivariate time series (SBS-MVTS) approach of Cho & Fryzlewicz (2015). For both methods, we report the locations of the estimated break points and the percentage of simulations where each break point is correctly identified. For our method, we also report the percentage of cases where the break point is correctly estimated in the R_n -radius of the truth.

For parameter estimation, we only evaluate the performance of our proposed method. Motivated by the EEG example of Section 1, we report true positive, false positive, true negative and false negative rates based on nonzero entries of the estimated coefficient matrices.

In order to apply the initial estimator 5, we need to select the tuning parameter λ_n . For finite number of break points m_0 , the rate for λ_n is discussed in Remark 1 of Section 4 as a function of n and p . However, this rate may not be applicable in finite sample simulations. Fortunately, our procedure is not sensitive to the choice of this tuning parameter: With smaller values of λ_n , more points are selected in the first stage; however, the additional break points are screened out in the second stage. Therefore, in this section, few values of λ_n were tried to find a reasonable range for this tuning parameter in each simulation scenario. The value of λ_n was then fixed for all of the 100 replications in each scenario.

Recall from Section 5 that for parameter estimation, we need to remove the selected break points together with their R_n -radius neighborhood in order to apply the proposed estimation in (15). In practice, the radius R_n needs to be estimated. A closer look at the proof of Theorem 4 together with Assumption A4 suggest that ω_n can be chosen as an upper bound for the selection radius R_n . In other words, in the statement of Theorem 4, the radius $Bm_0n\gamma_nd_n^{*2}$ can be replaced by ω_n and the result would still hold. Formally,

$$\mathbb{P} \left(\max_{1 \leq j \leq m_0} |\tilde{t}_j - t_j| \leq \omega_n \right) \rightarrow 1,$$

as $n \rightarrow \infty$. Therefore, in the simulation scenarios considered here, we set $R_n = \omega_n$. We also need to selection of the tuning parameter ρ_n for parameter estimation. To this end, we select ρ_n as the minimizer of the combined Bayesian Information Criterion (BIC) of all the remaining segments in the data. Following Lütkepohl (2005), for $j = 0, \dots, m_0$ we define the BIC on the interval $I_{j+1} = [r_{j2}, r_{(j+1)1}]$ as

$$\text{BIC}(j, \rho_n) = \log(\det \hat{\Sigma}_{\varepsilon, j}) + \frac{\log(r_{(j+1)1} - r_{j2})}{(r_{(j+1)1} - r_{j2})} \left\| \hat{\beta}_{j+1} \right\|_0,$$

where $\hat{\Sigma}_{\varepsilon, j}$ is the residual sample covariance matrix having used the estimated $\hat{\mathbf{B}}$ in Equation 15, and $\|\hat{\beta}_{j+1}\|_0$ is the number of non-zero elements in $\hat{\beta}_{j+1}$; then ρ_n is selected as

$$\hat{\rho}_n = \operatorname{argmin}_{\rho_n} \sum_{j=0}^{m_0} \text{BIC}(j, \rho_n). \quad (16)$$

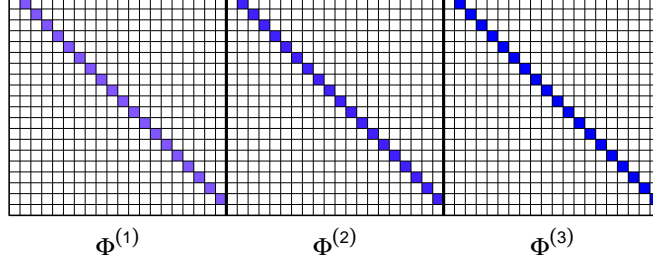


Figure 3: True autoregressive coefficients for the three segments used in the Simulation Scenario 1.

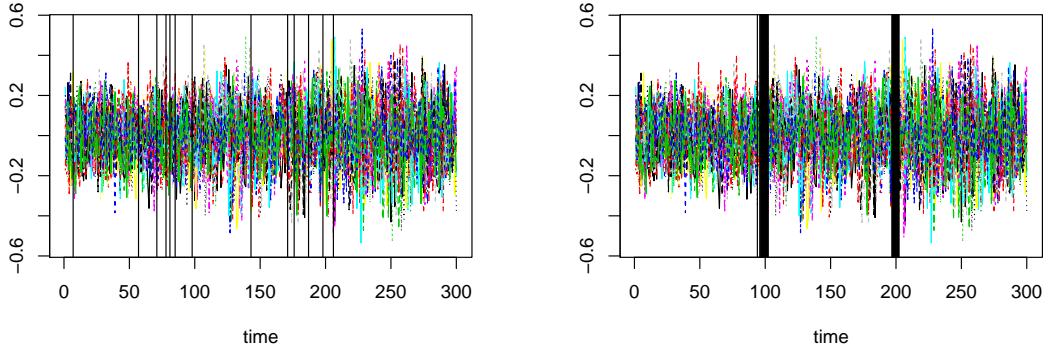


Figure 4: Left: Estimated break points from the first stage of the proposed procedure (Equation 5) for one of the runs in Simulation Scenario 1; on average ~ 13 points are selected in the first stage. Right: Final selected break points for all 100 simulation runs in Simulation Scenario 1.

Simulation Scenario 1 (Simple Φ and break points close to the center). In the first scenario, the autoregressive coefficients are chosen to have the same structure but different values as displayed in Figure 3. In this scenario, $t_1 = 100$ and $t_2 = 200$, which means the break points are not close to the boundaries.

Selected break points in one out of 100 simulated data sets are shown in the left panel of Figure 4. As expected from Theorem 3, more than 2 change points are detected using the first stage estimator. However, there are always points selected in a small neighborhood of true change points. The second stage screening procedure eliminates the extra candidate points leaving only the two closest points to the true change points. The final selected points in all 100 simulation runs are shown in the right panel of Figure 4. The mean and standard deviation of locations of selected points, relative to the sample size T , are shown in Table 1. (More specifically, the mean and standard deviation of \tilde{t}_1/T and \tilde{t}_2/T are reported in the table.) It can be seen from the results that the two stage procedure accurately detects both the number of break points, as well as their locations. The results also suggest that our proposed procedure produces more accurate estimates of the break points than the SBS-MVTS method of Cho & Fryzlewicz (2015).

The advantage of our method is more pronounced when comparing the percentage of times where the break points are correctly detected using each method. This percentage is calculated as the proportion of simulations, where selected break points are close to each of the true break points. A selected break point is counted as a ‘success’ for the first true break point, t_1 , if it is in the interval $[0, t_1 + 0.5(t_2 - t_1)]$; similarly, a selected break point is counted as a ‘success’ for the second true break point, t_2 , if it falls in the interval $[t_1 + 0.5(t_2 - t_1), T]$.

Simulation Scenario 2 (Simple Φ and break points close to the boundaries). The coefficient matrices in this simulation are similar to those in Scenario 1. However, in this simulation, the break points are closer to the boundaries. Specifically, $t_1 = 50$ and $t_2 = 250$.

The final selected points are shown in the left panel of Figure 5, and mean and standard deviation of the

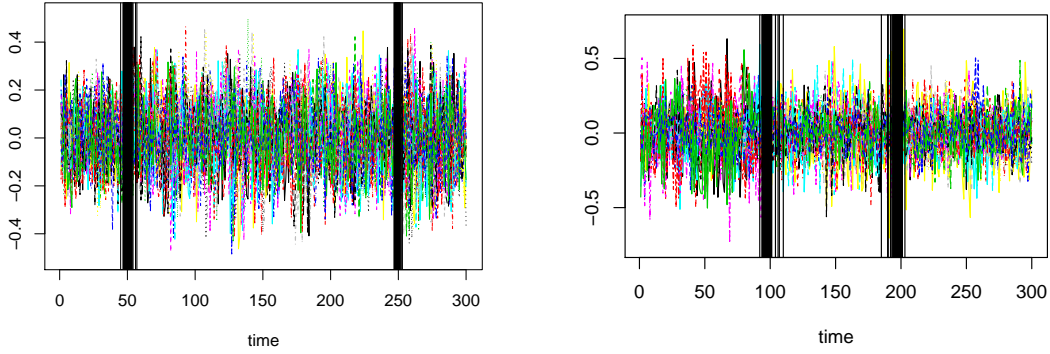


Figure 5: Final selected points for all 100 runs from Simulation Scenarios 2 (left) and 3 (right).

location of selected points, relative to the sample size T , and the percentage of times where the break points are correctly detected are shown in Table 2. The results indicate that as the break points get closer to the boundaries, the performance of the proposed procedure does not deviate much from Scenario 1. This is in stark contrast to SBS-MVTS, which gives worse estimates in this simulation setting.

Simulation Scenario 3 (Randomly structured Φ and break points close to the center). As in Scenario 1, in this case we set $t_1 = 100$ and $t_2 = 200$. However, the coefficients matrices are chosen to be randomly structured. As a result, detecting break points becomes more challenging in this setting. The autoregressive

method	break point	truth	mean	std	selection rate	R_n -radius selection rate
SBS-MVTS	1	0.3333	0.3513	0.039	0.85	–
	2	0.6667	0.6425	0.0558	0.87	–
Our method	1	0.3333	0.3306	0.0043	1	1
	2	0.6667	0.6646	0.0034	1	1

Table 1: Results for Simulation Scenario 1. The table shows mean and standard deviation of estimated break point locations, the percentage of simulation runs where break points are correctly detected, and the percentage of simulation runs where true break points are within the R_n -radius of the estimated break points.

method	break points	truth	mean	std	selection rate	R_n -radius selection rate
SBS-MVTS	1	0.1667	0.31	0.0802	0.94	–
	2	0.8333	0.6414	0.102	0.68	–
Our method	1	0.1667	0.1657	0.006	1	1
	2	0.8333	0.8305	0.0032	1	1

Table 2: Results for Simulation Scenario 2. The table shows mean and standard deviation of estimated break point locations, the percentage of simulation runs where break points are correctly detected, and the percentage of simulation runs where true break points are within the R_n -radius of the estimated break points.

method	break points	truth	mean	std	selection rate	R_n -radius selection rate
SBS-MVTS	1	0.3333	0.3238	0.0206	0.98	–
	2	0.6667	0.6569	0.0324	0.92	–
Our method	1	0.3333	0.3279	0.0082	0.99	0.98
	2	0.6667	0.6581	0.0088	1	0.96

Table 3: Results for Simulation Scenario 3. The table shows mean and standard deviation of estimated break point locations, the percentage of simulation runs where break points are correctly detected, and the percentage of simulation runs where true break points are within the R_n -radius of the estimated break points.

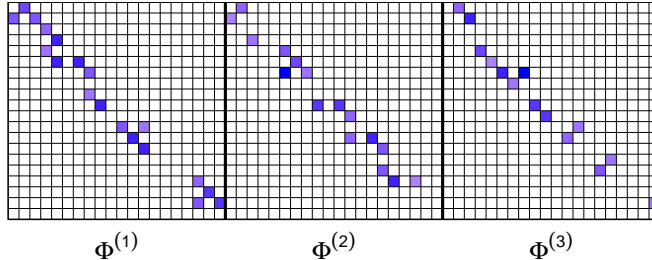


Figure 6: True autoregressive coefficients for the three segments used in the Simulation Scenario 3.

coefficients for this scenario are displayed in Figure 6.

The selected break points in this scenario are shown in right panel of Figure 5. The mean and standard deviation of locations of the selected break points, relative to the sample size T , as well as the percentage of simulation runs where break points are correctly identified are shown in Table 3. The results suggest that, among the three simulation scenarios, this setting, with randomly structured Φ 's, is the most challenging for our method. In this setting, the detection rate drops to 99% compared to 100% in scenario 1, and the standard deviation of the selected break point locations are almost doubled. The percentage of runs where the true break points are within the R_n -radius of the estimated points also drop to 96% compared to 100% in Scenarios 1 and 2.

The inferior performance of the proposed method in the third simulation scenario could be due to the fact that the L_2 distance between the consecutive autoregressive coefficients are less than the previous two cases. This would make it harder to identify the exact location of the break points. In contrast, the sparse changes in coefficient matrices makes this setting more favorable for SBS-MVTS. Nonetheless, estimates from our method are as good or better than those from SBS-MVTS.

Table 4 summarizes the simulation results for the autoregressive parameter estimation in all the three simulation scenarios. The table shows mean and standard deviation of relative estimation error REE, as well as true positive rate (TPR), true negative rate (TNR), false positive rate (FPR), and false negative rate (FNR) of the estimates. The results suggest that the method also performs well in terms of parameter estimation. One potential explanation for the increased false positive rate in this scenario is that the first and the third segment for parameter estimation have length less than 40 as compared to length around 90 in Scenarios 1 and 3. This shorter length makes it harder to estimate the parameters and correctly select zero and non-zero coefficients.

	REE	SD(REE)	TPR	TNR	FPR	FNR
Simulation 1	0.3019	0.0042	0.98	1	0	0.02
Simulation 2	0.655	0.0178	0.95	0.65	0.35	0.05
Simulation 3	0.3235	0.0283	0.96	0.98	0.02	0.04

Table 4: Results of parameter estimation for all three simulation scenarios. The table shows mean and standard deviation of relative estimation error REE, as well as true positive rate TPR, true negative rate TNR, false positive rate FPR, and false negative rate FNR.

7 Applications

7.1 EEG Data

In this section, we revisit the EEG data discussed in Section 1. Recall that the data consists of electroencephalogram (EEG) signals recorded at 18 locations on the scalp of a patient diagnosed with left temporal lobe epilepsy during an epileptic seizure. The sampling rate is 100 Hz and the total number of time points per EEG is $T = 22,768$ over 228 seconds. The time series for all 18 EEG channels are shown in Figure 1. The seizure was estimated to take place at $t = 85s$. Examining the EEG plots, it can be seen that the magnitude

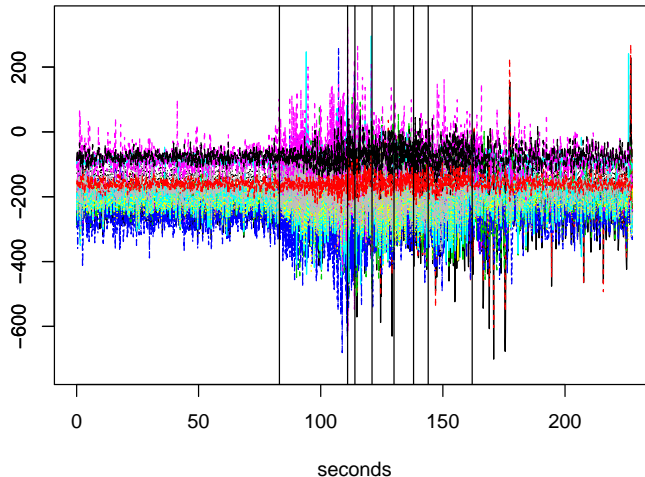


Figure 7: EEG data over 228 seconds with the 8 selected break points.

and the volatility of signals change simultaneously around that time. To speed up the computations, we selected ten observation per second and reduced the total time points to $T = 2276$.

Data from one of the EEG channels (P3) was previously used by Davis *et al.* (2006) and Chan *et al.* (2014) for detecting structural breaks in the time series. As a comparison, we apply the SBS-MVTS method of Cho & Fryzlewicz (2015) as well as our three-stage estimator to detect the break points based on changes in all 18 time series. Table 5 shows the location of the selected break points using the Auto-PARM method of Davis *et al.* (2006) and the two-stage procedure of Chan *et al.* (2014) based on data from channel P3, as well as those estimated using our method and SBS-MVTS based on all 18 channels. The selected break points by our method are also shown in Figure 7.

Our method detects a break point at $t = 83$, which is close to the seizure time identified by neurologists. The majority of other break points selected by our method are also close to the break points detected by the two univariate approaches and SBS-MVTS. However, the main advantage of our method is that it also provides consistent estimates of VAR parameters. As shown in Figure 2, these estimates can be used to glean novel insight into changes in mechanisms of interactions before and after seizure.

Given the proximity of selected break points between $t = 83$ and $t = 162$, in order to obtain the networks in Figure 2, we considered time series before and after these two time points. More specifically, using the procedure of Section 5, we discarded observations in the R_n radius before $t = 83$ and after $t = 162$ in order to ensure the stationarity of remaining observations. We then used the ℓ_1 -penalized least square estimator (15), with tuning parameter selected by BIC (16), to obtain estimates of VAR parameters before and after seizure. Edges in Figure 2 networks correspond to nonzero estimated coefficients that are at least larger than 0.05 in magnitude. This thresholding is motivated by the known over-selection property of lasso (Shojaie *et al.* 2012) and is used to improve the interpretability of estimated networks.

Methods	1	2	3	4	5	6	7	8	9	10	11
Auto-PARM	86	90	106	121	133	149	162	175	206	208	326
Chan (2014)	84	106	120	134	155	177	206	225	-	-	-
SBS-MVTS	84	107	114	126	133	143	157	176	-	-	-
Our method	83	111	114	121	130	138	144	162	-	-	-

Table 5: Location of break points detected in the EEG data using four estimation methods. The locations are rounded to the closest integer.

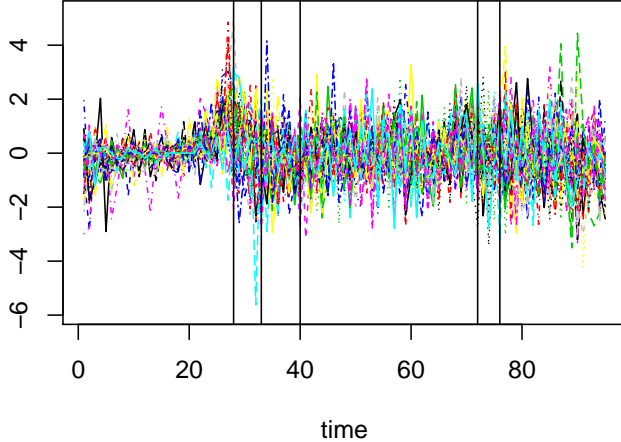


Figure 8: The NYC Yellow Cab Demand differenced time series from 39 different zipcodes over a single day with 96 time points. The 5 selected break points by the proposed method are shown as vertical lines.

7.2 Yellow Cab Demand in NYC

As a second example, we apply our method and SBS-MVTS to the yellow cab demand data in New York City (NYC), obtained from the NYC Taxi & Limousine Commission’s website¹. Here, the number of yellow cab pickups are aggregated spatially over the zipcodes and temporally over 15 minute intervals during April 16th, 2014. We only consider the zipcodes with more than 50 cab calls to obtain a better approximation using normal distribution. This results in 39 time series for zipcodes observed over 96 time points. To identify structural break points, we consider a differenced version of the data to remove first order non-stationarities.

Table 6 shows the 5 break points detected by our method, along with two break points identified by SBS-MVTS; the differenced time series and the detected break points are also shown in Figure 8. Based on data from NYC Metro (MTA), morning rush hour traffic in the city occurs between 6:30AM and 9:30AM, whereas the afternoon rush hour starts from 3:30PM and continues until 06:00PM. Interestingly, the selected break points are very close to the rush hour start/end times during a typical day. Specifically, the selected break points at 7AM, 10AM, and 6PM are close to rush hour periods in NYC. These results suggest that the covariance structure of cab demands between the zipcodes in NYC may significantly change before and after the rush hour periods. Even with the least conservative tuning parameters, SBS-MVTS only selects two break points, and does not identify any break points in the afternoon rush hour period.

	1	2	3	4	5
SBS-MVTS	6am	11:30am	–	–	–
Our method	7am	8:15am	10am	6pm	7pm

Table 6: The location of break points for the NYC Yellow Cab Demand data.

8 Discussion

In this article, we proposed a three-stage method for simultaneous detection of structural break points and parameter estimation in high-dimensional piecewise stationary VAR models.

We showed that the proposed method consistently detects the total number of the break points, and their locations. Moreover, it consistently estimates the parameters of high-dimensional sparse piecewise stationary VAR model. Numerical experiments in three simulation settings and two real data applications corroborate

¹<http://www.nyc.gov/html/tlc/html/about/trip-record-data.shtml>

these theoretical findings. In particular, in both real data examples considered, the break points detected using the proposed method are in agreement with the nature of the data sets.

When the total number of break points m_0 is finite, the rate of consistency for detecting break point locations relative to the sample size T is affected by three factors: (1) the number of time points T , (2) the number of time series observed p , (3) the total sparsity of the model d_n^* . For the univariate case, this rate was shown to be of order $(\log n)/n$ by Chan *et al.* (2014). In the high-dimensional case, the rate shown here is of order $(d_n^{*2} \log n \log p)/n$. The $\log p$ and d_n^* factors in this rate highlights the challenges of change point detection in high dimensions. The proposed procedure also allows the number of break points to increase with the sample size, as long as the minimum distance between consecutive break points is large enough, as characterized by Assumptions A3 and A4.

One limitation of the proposed procedure is the need to select multiple tuning parameter. Among these, selecting the penalty parameter for the second stage estimator (10) can be challenging in practice. In the numerical studies in this paper, a simplified version of this tuning parameter was used. However, this simplified version does not guarantee optimal rates of consistency for break point estimation. Investigating optimal choices of tuning parameters for the proposed procedure can thus be a fruitful area of future research.

References

- Aue, Alexander, Hörmann, Siegfried, Horváth, Lajos, Reimherr, Matthew, *et al.* . 2009. Break detection in the covariance structure of multivariate time series models. *The Annals of Statistics*, **37**(6B), 4046–4087.
- Bai, Jushan. 1997. Estimation of a change point in multiple regression models. *The review of economics and statistics*, **79**(4), 551–563.
- Basu, Sumanta, & Michailidis, George. 2015. Regularized estimation in sparse high-dimensional time series models. *The Annals of Statistics*, **43**(4), 1535–1567.
- Bickel, Peter J, Ritov, Yaacov, & Tsybakov, Alexandre B. 2009. Simultaneous analysis of LASSO and Dantzig selector. *The Annals of Statistics*, **37**(4), 1705–1732.
- Boysen, Leif, Kempe, Angela, Liebscher, Volkmar, Munk, Axel, & Wittich, Olaf. 2009. Consistencies and rates of convergence of jump-penalized least squares estimators. *The Annals of Statistics*, 157–183.
- Chan, Ngai Hang, Yau, Chun Yip, & Zhang, Rong-Mao. 2014. Group LASSO for structural break time series. *Journal of the American Statistical Association*, **109**(506), 590–599.
- Chen, Shizhe, Shojaie, Ali, & Witten, Daniela M. 2016. Network Reconstruction From High Dimensional Ordinary Differential Equations. *Journal of the American Statistical Association*.
- Chen, Shizhe, Witten, Daniela, & Shojaie, Ali. 2017. Nearly assumptionless screening for the mutually-exciting multivariate Hawkes process. *Electronic Journal of Statistics*, **11**(1), 1207–1234.
- Chen, Xiaohui, Xu, Mengyu, & Wu, Wei Biao. 2013. Covariance and precision matrix estimation for high-dimensional time series. *The Annals of Statistics*, **41**(6), 2994–3021.
- Cho, Haeran, & Fryzlewicz, Piotr. 2015. Multiple-change-point detection for high dimensional time series via sparsified binary segmentation. *Journal of the Royal Statistical Society: Series B (Statistical Methodology)*, **77**(2), 475–507.
- Cho, Haeran, *et al.* . 2016. Change-point detection in panel data via double CUSUM statistic. *Electronic Journal of Statistics*, **10**(2), 2000–2038.
- Clarida, Richard, Gali, Jordi, & Gertler, Mark. 2000. Monetary policy rules and macroeconomic stability: evidence and some theory. *The Quarterly journal of economics*, **115**(1), 147–180.
- Dahlhaus, Rainer. 2012. Locally stationary processes. *Handbook of statistics*, **30**, 351–412.
- Davis, Richard A, Lee, Thomas C M, & Rodriguez-Yam, Gabriel A. 2006. Structural break estimation for nonstationary time series models. *Journal of the American Statistical Association*, **101**(473), 223–239.

- De Mol, Christine, Giannone, Domenico, & Reichlin, Lucrezia. 2008. Forecasting using a large number of predictors: Is Bayesian shrinkage a valid alternative to principal components? *Journal of Econometrics*, **146**(2), 318–328.
- Ding, Xin, Qiu, Ziyi, & Chen, Xiaohui. 2016. Sparse transition matrix estimation for high-dimensional and locally stationary vector autoregressive models. *arXiv preprint arXiv:1604.04002*.
- Fan, Jianqing, Lv, Jinchi, & Qi, Lei. 2011. Sparse high-dimensional models in economics.
- Fujita, André, Sato, João R, Garay-Malpartida, Humberto M, Yamaguchi, Rui, Miyano, Satoru, Sogayar, Mari C, & Ferreira, Carlos E. 2007. Modeling gene expression regulatory networks with the sparse vector autoregressive model. *BMC Systems Biology*, **1**(1), 39.
- Granger, Clive WJ. 1969. Investigating causal relations by econometric models and cross-spectral methods. *Econometrica: Journal of the Econometric Society*, 424–438.
- Hall, Eric C, Raskutti, Garvesh, & Willett, Rebecca. 2016. Inference of High-dimensional Autoregressive Generalized Linear Models. *arXiv preprint arXiv:1605.02693*.
- Hansen, Niels Richard, Reynaud-Bouret, Patricia, & Rivoirard, Vincent. 2015. Lasso and probabilistic inequalities for multivariate point processes. *Bernoulli*, **21**(1), 83–143.
- Harchaoui, Zaid, & Lévy-Leduc, Céline. 2010. Multiple change-point estimation with a total variation penalty. *Journal of the American Statistical Association*, **105**(492), 1480–1493.
- Loh, Po-Ling, & Wainwright, Martin J. 2012. High-dimensional regression with noisy and missing data: Provable guarantees with nonconvexity. *Ann. Statist.*, **40**(3), 1637–1664.
- Lu, Tao, Liang, Hua, Li, Hongzhe, & Wu, Hulin. 2011. High-dimensional ODEs coupled with mixed-effects modeling techniques for dynamic gene regulatory network identification. *Journal of the American Statistical Association*, **106**(496), 1242–1258.
- Lütkepohl, Helmut. 2005. *New introduction to multiple time series analysis*. Springer Science & Business Media.
- Michailidis, George, & dAlché Buc, Florence. 2013. Autoregressive models for gene regulatory network inference: Sparsity, stability and causality issues. *Mathematical biosciences*, **246**(2), 326–334.
- Mukhopadhyay, Nitai D, & Chatterjee, Snigdhanu. 2006. Causality and pathway search in microarray time series experiment. *Bioinformatics*, **23**(4), 442–449.
- Nicholson, William B, Matteson, David S, & Bien, Jacob. 2017. VARX-L: Structured regularization for large vector autoregressions with exogenous variables. *International Journal of Forecasting*, **33**(3), 627–651.
- Ombao, Hernando, Von Sachs, Rainer, & Guo, Wensheng. 2005. SLEX analysis of multivariate nonstationary time series. *Journal of the American Statistical Association*, **100**(470), 519–531.
- Primiceri, Giorgio E. 2005. Time varying structural vector autoregressions and monetary policy. *The Review of Economic Studies*, **72**(3), 821–852.
- Qiu, Huitong, Han, Fang, Liu, Han, & Caffo, Brian. 2016. Joint estimation of multiple graphical models from high dimensional time series. *Journal of the Royal Statistical Society: Series B (Statistical Methodology)*, **78**(2), 487–504.
- Sato, João R, Morettin, Pedro A, Arantes, Paula R, & Amaro, Edson. 2007. Wavelet based time-varying vector autoregressive modelling. *Computational Statistics & Data Analysis*, **51**(12), 5847–5866.
- Shojaie, A., & Michailidis, G. 2010. Discovering graphical Granger causality using the truncating lasso penalty. *Bioinformatics*, **26**(18), i517–i523.

- Shojaie, A., Basu, S., & Michailidis, G. 2012. Adaptive thresholding for reconstructing regulatory networks from time-course gene expression data. *Statistics in Biosciences*, **4**(1), 66–83.
- Smith, Stephen M. 2012. The future of fMRI connectivity. *Neuroimage*, **62**(2), 1257–1266.
- Tank, Alex, Foti, Nicholas J, & Fox, Emily B. 2015. Bayesian structure learning for stationary time series. *Pages 872–881 of: Proceedings of the Thirty-First Conference on Uncertainty in Artificial Intelligence*. AUAI Press.
- Tseng, Paul, & Yun, Sangwoon. 2009. A coordinate gradient descent method for nonsmooth separable minimization. *Mathematical Programming*, **117**(1), 387–423.
- Xiao, Han, & Wu, Wei Biao. 2012. Covariance matrix estimation for stationary time series. *The Annals of Statistics*, **40**(1), 466–493.

Appendix

This section collects the technical lemmas, as well as the proofs of the main results in the paper.

Appendix A: Technical Lemmas

Lemma 1. *There exist constants $c_i > 0$ such that for $n \geq c_0 (\log(n) + 2 \log(p) + \log(q))$, with probability at least $1 - c_1 \exp(-c_2 (\log(n) + 2 \log(p) + \log(q)))$, we have*

$$\left\| \frac{\mathbf{Z}' \mathbf{E}}{n} \right\|_{\infty} \leq c_3 \sqrt{\frac{\log(n) + 2 \log(p) + \log(q)}{n}} \quad (17)$$

Proof. Note that $\frac{1}{n} \mathbf{Z}' \mathbf{E} = \frac{1}{n} (I_p \otimes \mathcal{X}') \mathbf{E} = \text{vec}(\mathcal{X}' E) / n$. Let $\mathcal{X}(h, \cdot)$ and $\mathcal{X}(h, l)$ be the h -th block column and the l -th column of the h -th block column of \mathcal{X} , respectively, $1 \leq h \leq n$, $1 \leq l \leq d$. More specifically,

$$\mathcal{X}(h, \cdot) = \begin{pmatrix} 0 \\ \vdots \\ 0 \\ y'_{q+h-2} & \cdots & y'_{h-1} \\ \vdots \\ y'_{T-1} & \cdots & y'_{T-q} \end{pmatrix}_{n \times pq}, \quad \mathcal{X}(h, l) = \begin{pmatrix} 0 \\ \vdots \\ 0 \\ y'_{q+h-l-1} \\ \vdots \\ y'_{T-l} \end{pmatrix}_{n \times p}. \quad (18)$$

Now,

$$\left\| \frac{\mathbf{Z}' \mathbf{E}}{n} \right\|_{\infty} = \max_{1 \leq h \leq n, 1 \leq l \leq d, 1 \leq i, j \leq p} \left| e'_i \left(\frac{\mathcal{X}'(h, l) E}{n} \right) e_j \right|, \quad (19)$$

where $e_i \in \mathbb{R}^p$ with the i -th element equals to 1 and zero on the rest. Note that,

$$\frac{\mathcal{X}'(h, l) E}{n} = \frac{1}{n} \sum_{t=h-l-1}^{T-q-l} y_{q+t} \varepsilon'_{q+t+l}.$$

Now, since $\text{cov}(y_{q+t}, \varepsilon_{q+t+l}) = 0$ for all t, l, h , similar argument as in Proposition 2.4(b) of Basu & Michailidis (2015) shows that for fixed i, j, h, l , there exist $k_1, k_2 > 0$ such that for all $\eta > 0$:

$$\mathbb{P} \left(\left| e'_i \left(\frac{\mathcal{X}'(h, l) E}{n} \right) e_j \right| > k_1 \eta \right) \leq 6 \exp(-k_2 n \min(\eta, \eta^2)).$$

Set $\eta = k_3 \sqrt{\frac{\log(n) + 2 \log(p) + \log(q)}{n}}$ for a large enough $k_3 > 0$, and taking the union over the $\pi = np^2q$ possible choices of i, j, h, l yield the result. \square

Lemma 2. *Let $\hat{\Theta}$ be defined as in (5), then under the assumptions of Theorem 1:*

$$\sum_{l=\hat{t}_j}^n Y_{l-1} \left(y'_l - Y'_{l-1} \sum_{i=1}^l \hat{\theta}'_i \right) = \frac{n \lambda_n}{2} \text{sign}(\hat{\theta}'_{\hat{t}_j}), \quad \text{for } j = 1, 2, \dots, \hat{m}, \quad (20)$$

where $Y'_l = (y'_l \cdots y'_{l-q+1})_{1 \times pq}$, and

$$\left\| \sum_{l=j}^n Y_{l-1} \left(y'_l - Y'_{l-1} \sum_{i=1}^l \hat{\theta}'_i \right) \right\|_{\infty} \leq \frac{n \lambda_n}{2}, \quad \text{for } j = q-1, 2, \dots, n. \quad (21)$$

Moreover, $\sum_{i=1}^t \hat{\theta}_i = \hat{\Phi}^{(\cdot, j)}$ for $\hat{t}_{j-1} \leq t \leq \hat{t}_j - 1$, $j = 1, 2, \dots, |\mathcal{A}_n|$.

Proof. This is just checking the KKT condition of the proposed optimization problem. \square

Lemma 3. Under assumption A1, there exist constants $c_i > 0$ such that with probability at least $1 - c_1 \exp(-c_2(\log(q) + 2\log(p)))$,

$$\sup_{1 \leq j \leq m_0, s \geq t_j, |t_j - s| > n\gamma_n} \left\| (t_j - s)^{-1} \left(\sum_{l=s}^{t_j-1} Y_{l-1} Y'_{l-1} - \Gamma_j^q(0) \right) \right\|_{\infty} \leq c_3 \sqrt{\frac{\log(q) + 2\log(p)}{n\gamma_n}}, \quad (22)$$

where $\Gamma_j^q(0) = \mathbb{E}(Y_{l-1} Y'_{l-1})$, and

$$\sup_{1 \leq j \leq m_0, s \geq t_j, |t_j - s| > n\gamma_n} \left\| (t_j - s)^{-1} \sum_{l=s}^{t_j-1} Y_{l-1} \varepsilon'_l \right\|_{\infty} \leq c_3 \sqrt{\frac{\log(q) + 2\log(p)}{n\gamma_n}}. \quad (23)$$

Proof. The proof of this lemma is similar to Proposition 2.4 in Basu & Michailidis (2015). Here we briefly mention the proof omitting the details. For the first one, note that using similar argument as in Proposition 2.4(a) in Basu & Michailidis (2015), there exist $k_1, k_2 > 0$ such that for each fixed $k, l = 1, \dots, pq$,

$$\mathbb{P} \left(\left| e'_k \frac{\sum_{l=s}^{t_j-1} Y_{l-1} Y'_{l-1} - \Gamma_j^q(0)}{t_j - s} e_l \right| > k_1 \eta \right) \leq 6 \exp(-k_2 n\gamma_n \min(\eta, \eta^2)). \quad (24)$$

Setting $\eta = k_3 \sqrt{\frac{\log(qp^2)}{n\gamma_n}}$, and taking the union over all possible values of k, l , we get the first part. For the second part, the proof will be similar to lemma (1). Again, there exist $k_1, k_2 > 0$ such that for each fixed $k = 1, \dots, pq, l = 1, \dots, p$,

$$\mathbb{P} \left(\left| e'_k \frac{\sum_{l=s}^{t_j-1} Y_{l-1} \varepsilon'_l}{t_j - s} e_l \right| > k_1 \eta \right) \leq 6 \exp(-k_2 n\gamma_n \min(\eta, \eta^2)). \quad (25)$$

Setting $\eta = k_3 \sqrt{\frac{\log(qp^2)}{n\gamma_n}}$, and taking the union over all possible values of k, l , we get:

$$\left\| (t_j - s)^{-1} \left(\sum_{l=s}^{t_j-1} Y_{l-1} Y'_{l-1} - \Gamma_j^q(0) \right) \right\|_{\infty} \leq c_3 \sqrt{\frac{\log(q) + 2\log(p)}{n\gamma_n}}, \quad (26)$$

and

$$\left\| (t_j - s)^{-1} \sum_{l=s}^{t_j-1} Y_{l-1} \varepsilon'_l \right\|_{\infty} \leq c_3 \sqrt{\frac{\log(q) + 2\log(p)}{n\gamma_n}}, \quad (27)$$

with high probability converging to 1 for any $j = 1, 2, \dots, m_0$, as long as $|t_j - s| > n\gamma_n$ and $s \geq t_{j-1}$. Note that the constants c_1, c_2, c_3 can be chosen large enough and in such a way that the upper bounds above would be independent of the break point t_i . Therefore, we have the desired upper bounds verified with probability at least $1 - c_1 \exp(-c_2(\log(q) + 2\log(p)))$. \square

Lemma 4. Under the assumptions of Theorem 4, for $m < m_0$, there exist constants $c_1, c_2 > 0$ such that:

$$\mathbb{P} \left(\min_{(s_1, \dots, s_m) \subset \{1, \dots, T\}} L_n(s_1, s_2, \dots, s_m; \eta_n) > \sum_{t=q}^T \|\varepsilon_t\|_2^2 + c_1 \Delta_n - c_2 m n \gamma_n d_n^{*2} \right) \rightarrow 1, \quad (28)$$

where $\Delta_n = \min_{1 \leq j \leq m_0+1} |t_j - t_{j-1}|$.

Proof. Since $m < m_0$, there exists a point t_j such that $|s_i - t_j| > \Delta_n/4$. In order to find a lower bound on the sum of the least squares, we consider three different cases: (a) $|s_i - s_{i-1}| \leq n\gamma_n$; (b) There exist two true break points t_j, t_{j+1} such that $|s_{i-1} - t_j| \leq n\gamma_n$ and $|s_i - t_{j+1}| \leq n\gamma_n$; (c) Otherwise. The idea is to find a lower bound for the sum of squared errors plus the penalty term for each case. Here, we consider only one candidate for each case. The general case can be argued similarly, but omitted here to avoid complex notations. Denote the estimated parameter in each of the estimated segments below by $\hat{\theta}$.

For case (a), consider the case where the interval (s_{i-1}, s_i) is inside a true segment. In other words, there exists j such that $t_j < s_{i-1} < s_i < t_{j+1}$. Now,

$$\begin{aligned}
\sum_{t=s_{i-1}}^{s_i-1} \|y_t - \widehat{\theta} Y_{t-1}\|_2^2 &= \sum_{t=s_{i-1}}^{s_i-1} \|\varepsilon_t\|_2^2 + \sum_{t=s_{i-1}}^{s_i-1} \|(\Phi^{(\cdot, j+1)} - \widehat{\theta}) Y_{t-1}\|_2^2 \\
&+ 2 \sum_{t=s_{i-1}}^{s_i-1} Y'_{t-1} (\Phi^{(\cdot, j+1)} - \widehat{\theta})' \varepsilon_t \\
&\geq \sum_{t=s_{i-1}}^{s_i-1} \|\varepsilon_t\|_2^2 + 0 - \left| 2 \sum_{t=s_{i-1}}^{s_i-1} Y'_{t-1} (\Phi^{(\cdot, j+1)} - \widehat{\theta})' \varepsilon_t \right| \\
&\geq \sum_{t=s_{i-1}}^{s_i-1} \|\varepsilon_t\|_2^2 - c\sqrt{n\gamma_n \log p} \|\Phi^{(\cdot, j+1)} - \widehat{\theta}\|_1, \tag{29}
\end{aligned}$$

and therefore, based on the tuning parameter selected based on Assumption A4, we have:

$$\sum_{t=s_{i-1}}^{s_i-1} \|y_t - \widehat{\theta} Y_{t-1}\|_2^2 + \eta_{(s_{i-1}, s_i)} \|\widehat{\theta}\|_1 \geq \sum_{t=s_{i-1}}^{s_i-1} \|\varepsilon_t\|_2^2 - c\sqrt{n\gamma_n \log p} \|\Phi^{(\cdot, j+1)}\|_1. \tag{30}$$

For case (b), consider the case where $s_{i-1} < t_j$ and $s_i < t_{j+1}$. Now, similar arguments as in Proposition 4.1 in Basu & Michailidis (2015) show that by the tuning parameter selected based on A4 (b), we have:

$$\|\Phi^{(\cdot, j+1)} - \widehat{\theta}\|_1 \leq 4\sqrt{d_n^*} \|\Phi^{(\cdot, j+1)} - \widehat{\theta}\|_2, \text{ and } \|\Phi^{(\cdot, j+1)} - \widehat{\theta}\|_2 \leq c_3\sqrt{d_n^*} \eta_{(s_{i-1}, s_i)}. \tag{31}$$

To see this, observe that based on the definition of $\widehat{\theta}$, it will beat any other choice including $\Phi^{(\cdot, j+1)}$. Therefore,

$$\frac{1}{s_i - s_{i-1}} \sum_{t=s_{i-1}}^{s_i-1} \|y_t - \widehat{\theta} Y_{t-1}\|_2^2 + \eta_{(s_{i-1}, s_i)} \|\widehat{\theta}\|_1 \leq \frac{1}{s_i - s_{i-1}} \sum_{t=s_{i-1}}^{s_i-1} \|y_t - \Phi^{(\cdot, j+1)} Y_{t-1}\|_2^2 + \eta_{(s_{i-1}, s_i)} \|\Phi^{(\cdot, j+1)}\|_1. \tag{32}$$

Some rearrangements lead to:

$$\begin{aligned}
0 \leq c' \|\Phi^{(\cdot, j+1)} - \widehat{\theta}\|_2^2 &\leq \frac{1}{s_i - s_{i-1}} \sum_{t=s_{i-1}}^{s_i-1} Y'_{t-1} (\Phi^{(\cdot, j+1)} - \widehat{\theta})' (\Phi^{(\cdot, j+1)} - \widehat{\theta}) Y_{t-1} \\
&\leq \frac{2}{s_i - s_{i-1}} \sum_{t=s_{i-1}}^{s_i-1} Y'_{t-1} (\Phi^{(\cdot, j+1)} - \widehat{\theta})' (y_t - \Phi^{(\cdot, j+1)} Y_{t-1}) + \eta_{(s_{i-1}, s_i)} (\|\Phi^{(\cdot, j+1)}\|_1 - \|\widehat{\theta}\|_1) \\
&\leq \left(c\sqrt{\frac{\log p}{s_i - s_{i-1}}} + M_\Phi d_n^* \frac{n\gamma_n}{s_i - s_{i-1}} \right) \|\Phi^{(\cdot, j+1)} - \widehat{\theta}\|_1 + \eta_{(s_{i-1}, s_i)} (\|\Phi^{(\cdot, j+1)}\|_1 - \|\widehat{\theta}\|_1) \\
&\leq \frac{\eta_{(s_{i-1}, s_i)}}{2} \|\Phi^{(\cdot, j+1)} - \widehat{\theta}\|_1 + \eta_{(s_{i-1}, s_i)} (\|\Phi^{(\cdot, j+1)}\|_1 - \|\widehat{\theta}\|_1) \\
&\leq \frac{3\eta_{(s_{i-1}, s_i)}}{2} \|\Phi^{(\cdot, j+1)} - \widehat{\theta}\|_{1, \mathcal{I}} - \frac{\eta_{(s_{i-1}, s_i)}}{2} \|\Phi^{(\cdot, j+1)} - \widehat{\theta}\|_{1, \mathcal{I}^c} \\
&\leq 2\eta_{(s_{i-1}, s_i)} \|\Phi^{(\cdot, j+1)} - \widehat{\theta}\|_1, \tag{33}
\end{aligned}$$

and this ensures that $\|\Phi^{(\cdot, j+1)} - \widehat{\theta}\|_{1, \mathcal{I}^c} \leq 3\|\Phi^{(\cdot, j+1)} - \widehat{\theta}\|_{1, \mathcal{I}}$, and hence $\|\Phi^{(\cdot, j+1)} - \widehat{\theta}\|_1 \leq 4\|\Phi^{(\cdot, j+1)} - \widehat{\theta}\|_{1, \mathcal{I}} \leq 4\sqrt{d_n^*} \|\Phi^{(\cdot, j+1)} - \widehat{\theta}\|_2$. This comparison between L_1 and L_2 norms of the error term together with the bound in equation 33 will get the desired consistency rates.

Similar to case (a), using lemma (3), we have:

$$\begin{aligned}
\sum_{t=t_j}^{s_i-1} \|y_t - \widehat{\theta} Y_{t-1}\|_2^2 &\geq \sum_{t=t_j}^{s_i-1} \|\varepsilon_t\|_2^2 + c|s_i - t_j| \|\Phi^{(\cdot, j+1)} - \widehat{\theta}\|_2^2 - c' \sqrt{|s_i - t_j| \log p} \|\Phi^{(\cdot, j+1)} - \widehat{\theta}\|_1 \\
&\geq \sum_{t=t_j}^{s_i-1} \|\varepsilon_t\|_2^2 + c|s_i - t_j| \|\Phi^{(\cdot, j+1)} - \widehat{\theta}\|_2 \left(\|\Phi^{(\cdot, j+1)} - \widehat{\theta}\|_2 - \frac{c'}{c} \sqrt{\frac{d_n^* \log p}{|s_i - t_j|}} \right) \\
&\geq \sum_{t=t_j}^{s_i-1} \|\varepsilon_t\|_2^2 - c' d_n^* \log p.
\end{aligned} \tag{34}$$

Also, for the interval (s_{i-1}, t_j) , we have:

$$\begin{aligned}
\sum_{t=s_{i-1}}^{t_j-1} \|y_t - \widehat{\theta} Y_{t-1}\|_2^2 &\geq \sum_{t=s_{i-1}}^{t_j-1} \|\varepsilon_t\|_2^2 - c' \sqrt{n\gamma_n \log p} \|\Phi^{(\cdot, j)} - \widehat{\theta}\|_1 \\
&\geq \sum_{t=s_{i-1}}^{t_j-1} \|\varepsilon_t\|_2^2 - c' \sqrt{n\gamma_n \log p} \left(\|\Phi^{(\cdot, j+1)} - \widehat{\theta}\|_1 + \|\Phi^{(\cdot, j+1)} - \Phi^{(\cdot, j)}\|_1 \right) \\
&\geq \sum_{t=s_{i-1}}^{t_j-1} \|\varepsilon_t\|_2^2 - c' \sqrt{n\gamma_n \log p} \left(d_n^* \eta_{(s_{i-1}, s_i)} + \|\Phi^{(\cdot, j+1)} - \Phi^{(\cdot, j)}\|_1 \right) \\
&\geq \sum_{t=s_{i-1}}^{t_j-1} \|\varepsilon_t\|_2^2 - c' d_n^* \sqrt{n\gamma_n \log p},
\end{aligned} \tag{35}$$

which in total by combining equations (34) and (35) gives:

$$\sum_{t=s_{i-1}}^{s_i-1} \|y_t - \widehat{\theta} Y_{t-1}\|_2^2 \geq \sum_{t=s_{i-1}}^{s_i-1} \|\varepsilon_t\|_2^2 - c' d_n^* \sqrt{n\gamma_n \log p}. \tag{36}$$

For case (c), consider the case where $s_{i-1} < t_j < s_i$ with $|s_{i-1} - t_j| > \Delta_n/4$ and $|s_i - t_j| > \Delta_n/4$. Similar arguments as in Proposition 4.1 of Basu & Michailidis (2015) shows that :

$$\|\Phi^{(\cdot, j+1)} - \widehat{\theta}\|_1 \leq 4\sqrt{d_n^*} \|\Phi^{(\cdot, j+1)} - \widehat{\theta}\|_2, \text{ and } \|\Phi^{(\cdot, j)} - \widehat{\theta}\|_1 \leq 4\sqrt{d_n^*} \|\Phi^{(\cdot, j)} - \widehat{\theta}\|_2. \tag{37}$$

Note that in this case, the restricted eigenvalue doesn't hold and therefore, the convergence of the $\widehat{\theta}$ cannot be verified. The reason is that in this case, the two parts of the true segments which intersect with the estimated segment have large lengths. If the length of one of them was negligible as compared to the other segment, one could still verify the restricted eigenvalue, but that's not the case here. However, the deterministic part of the deviation bound argument holds with the suitable choice of the tuning parameter. Now, similar to case (b), we have on both intervals (s_{i-1}, t_j) and (t_j, s_i) :

$$\begin{aligned}
\sum_{t=s_{i-1}}^{t_j-1} \|y_t - \widehat{\theta} Y_{t-1}\|_2^2 &\geq \sum_{t=s_{i-1}}^{t_j-1} \|\varepsilon_t\|_2^2 + c|t_j - s_{i-1}| \|\Phi^{(\cdot, j)} - \widehat{\theta}\|_2^2 - c' \sqrt{|t_j - s_{i-1}| \log p} \|\Phi^{(\cdot, j)} - \widehat{\theta}\|_1 \\
&\geq \sum_{t=s_{i-1}}^{t_j-1} \|\varepsilon_t\|_2^2 + c|t_j - s_{i-1}| \|\Phi^{(\cdot, j)} - \widehat{\theta}\|_2 \left(\|\Phi^{(\cdot, j)} - \widehat{\theta}\|_2 - \frac{c'}{c} \sqrt{\frac{d_n^* \log p}{|t_j - s_{i-1}|}} \right)
\end{aligned} \tag{38}$$

and

$$\begin{aligned}
\sum_{t=t_j}^{s_i-1} \|y_t - \widehat{\theta} Y_{t-1}\|_2^2 &\geq \sum_{t=t_j}^{s_i-1} \|\varepsilon_t\|_2^2 + c|s_i - t_j| \|\Phi^{(\cdot, j+1)} - \widehat{\theta}\|_2^2 - c' \sqrt{|s_i - t_j| \log p} \|\Phi^{(\cdot, j+1)} - \widehat{\theta}\|_1 \\
&\geq \sum_{t=t_j}^{s_i-1} \|\varepsilon_t\|_2^2 + c|s_i - t_j| \|\Phi^{(\cdot, j+1)} - \widehat{\theta}\|_2 \left(\|\Phi^{(\cdot, j+1)} - \widehat{\theta}\|_2 - \frac{c'}{c} \sqrt{\frac{d_n^* \log p}{|s_i - t_j|}} \right).
\end{aligned} \tag{39}$$

Now, since $\|\Phi^{(\cdot, j+1)} - \Phi^{(\cdot, j)}\|_2 \geq v > 0$, either $\|\Phi^{(\cdot, j+1)} - \widehat{\theta}\|_2 \geq v/4$ or $\|\Phi^{(\cdot, j)} - \widehat{\theta}\|_2 \geq v/4$. Assume that $\|\Phi^{(\cdot, j)} - \widehat{\theta}\|_2 \geq v/4$. Then, based on equation 38, we get for some $c_1 > 0$:

$$\sum_{t=s_{i-1}}^{t_j-1} \|y_t - \widehat{\theta}Y_{t-1}\|_2^2 \geq \sum_{t=s_{i-1}}^{t_j-1} \|\varepsilon_t\|_2^2 + c_1\Delta_n. \quad (40)$$

Moreover, for the second interval we get:

$$\sum_{t=t_j}^{s_i-1} \|y_t - \widehat{\theta}Y_{t-1}\|_2^2 \geq \sum_{t=t_j}^{s_i-1} \|\varepsilon_t\|_2^2 - c'd_n^* \log p, \quad (41)$$

which putting equations (40) and (41) together leads to:

$$\sum_{t=s_{i-1}}^{s_i-1} \|y_t - \widehat{\theta}Y_{t-1}\|_2^2 \geq \sum_{t=s_{i-1}}^{s_i-1} \|\varepsilon_t\|_2^2 + c_1\Delta_n - c'd_n^* \log p. \quad (42)$$

It is worth noting that there might be another situation in this case where $|s_{i-1} - t_j| > n\gamma_n$ and $|s_i - t_j| > n\gamma_n$. In this case, by using similar arguments as above we have the following lower bound:

$$\sum_{t=s_{i-1}}^{s_i-1} \|y_t - \widehat{\theta}Y_{t-1}\|_2^2 \geq \sum_{t=s_{i-1}}^{s_i-1} \|\varepsilon_t\|_2^2 - c'd_n^{*2} n\gamma_n. \quad (43)$$

Putting all of the cases together will yield the result. \square

Appendix B: Proof of Main Results

Proof of Theorem 1. By definition of $\widehat{\Theta}$, we get

$$\frac{1}{n} \|\mathbf{Y} - \mathbf{Z}\widehat{\Theta}\|_2^2 + \lambda_n \sum_{i=1}^n \|\widehat{\theta}_i\|_1 \leq \frac{1}{n} \|\mathbf{Y} - \mathbf{Z}\Theta\|_2^2 + \lambda_n \sum_{i=1}^n \|\theta_i\|_1. \quad (44)$$

Denoting $\mathcal{A} = \{t_1, t_1, \dots, t_{m_0}\}$, we have:

$$\begin{aligned} \frac{1}{n} \left\| \mathbf{Z} \left(\widehat{\Theta} - \Theta \right) \right\|_2^2 &\leq \frac{2}{n} \left(\widehat{\Theta} - \Theta \right)' \mathbf{Z}' \mathbf{E} + \lambda_n \sum_{i=1}^n \|\widehat{\theta}_i\|_1 - \lambda_n \sum_{i=1}^n \|\theta_i\|_1 \\ &\leq 2 \left\| \frac{\mathbf{Z}' \mathbf{E}}{n} \right\|_\infty \sum_{i=1}^n \|\theta_i - \widehat{\theta}_i\|_1 + \lambda_n \sum_{i \in \mathcal{A}} \left(\|\theta_i\|_1 - \|\widehat{\theta}_i\|_1 \right) - \lambda_n \sum_{i \in \mathcal{A}^c} \|\widehat{\theta}_i\|_1 \\ &\leq \lambda_n \sum_{i \in \mathcal{A}} \|\theta_i - \widehat{\theta}_i\|_1 + \lambda_n \sum_{i \in \mathcal{A}} \left(\|\theta_i\|_1 - \|\widehat{\theta}_i\|_1 \right) \\ &\leq 2\lambda_n \sum_{i \in \mathcal{A}} \|\theta_i\|_1 \\ &\leq 2\lambda_n m_n \max_{1 \leq j \leq m_0+1} \left\| \Phi^{(\cdot, j)} - \Phi^{(\cdot, j-1)} \right\|_1 \\ &\leq 4Cm_n \max_{1 \leq j \leq m_0+1} \left\{ \sum_{k=1}^p (d_{kj} + d_{k(j-1)}) \right\} M_\Phi \sqrt{\frac{\log(n) + 2\log(p) + \log(q)}{n}}, \end{aligned} \quad (45)$$

with high probability approaching to 1 due to Lemma 1. \square

Proof of Theorem 2. The proof is similar to Theorem 2.2 in Chan *et al.* (2014) and Proposition 5 in Harchaoui & Lévy-Leduc (2010). Before we start, define for a matrix $A \in \mathbb{R}^{pq \times p}$, $\|A\|_{\infty, \mathcal{I}} = \max_{j \in \mathcal{I}, 1 \leq k \leq p} |a_{jk}|$.

Now, if for some $j = 1, \dots, m_0$, $|\widehat{t}_j - t_j| > n\gamma_n$, this means that there exists a true break point t_{j_0} which is isolated from all the estimated points, i.e. $\min_{1 \leq j \leq m_0} |\widehat{t}_j - t_{j_0}| > n\gamma_n$. In other words, there exists an estimated break point \widehat{t}_j such that, $t_{j_0} - t_{j_0-1} \vee \widehat{t}_j \geq n\gamma_n$ and $t_{j_0+1} \wedge \widehat{t}_{j+1} \geq n\gamma_n$. By applying the second part of lemma (2) on the endpoints $t_{j_0-1} \vee \widehat{t}_j, t_{j_0}, t_{j_0+1} \wedge \widehat{t}_{j+1}$, and further using the triangular inequality, we get:

$$\left\| \sum_{l=t_{j_0-1} \vee \widehat{t}_j}^{t_{j_0}-1} Y_{l-1} Y'_{l-1} \left(\Phi^{(\cdot, j_0)} - \widehat{\Phi}^{(\cdot, j+1)} \right) \right\|_{\infty, \mathcal{I}} \leq n\lambda_n + \left\| \sum_{l=t_{j_0-1} \vee \widehat{t}_j}^{t_{j_0}-1} Y_{l-1} \varepsilon'_l \right\|_{\infty} \quad (46)$$

and

$$\left\| \sum_{l=t_{j_0}}^{t_{j_0+1} \wedge \widehat{t}_{j+1}-1} Y_{l-1} Y'_{l-1} \left(\Phi^{(\cdot, j_0+1)} - \widehat{\Phi}^{(\cdot, j+1)} \right) \right\|_{\infty, \mathcal{I}} \leq n\lambda_n + \left\| \sum_{l=t_{j_0}}^{t_{j_0+1} \wedge \widehat{t}_{j+1}-1} Y_{l-1} \varepsilon'_l \right\|_{\infty}. \quad (47)$$

Now, consider the first equation (46). We can write the left hand side as

$$(t_{j_0} - t_{j_0-1} \vee \widehat{t}_j)^{-1} \left\| \sum_{l=t_{j_0-1} \vee \widehat{t}_j}^{t_{j_0}-1} Y_{l-1} Y'_{l-1} \left(\Phi^{(\cdot, j_0)} - \widehat{\Phi}^{(\cdot, j+1)} \right) \right\|_{\infty, \mathcal{I}} \geq \left\| (\Gamma_{j_0}^q(0) - A) \left(\Phi^{(\cdot, j_0)} \right) \right\|_{\infty, \mathcal{I}} - \left\| (\Gamma_{j_0}^q(0) - A) \left(\widehat{\Phi}^{(\cdot, j+1)} \right) \right\|_{\infty} \quad (48)$$

for some random matrix A . Based on Lemma 3, it can be seen that $\|A\|_{\infty} \rightarrow 0$ with high probability converging to one. Then, we can show that based on the properties of the covariance matrix $\Gamma_{j_0}^q(0)$ that:

$$\left\| (\Gamma_{j_0}^q(0) - A) \left(\Phi^{(\cdot, j_0)} \right) \right\|_{\infty, \mathcal{I}} \geq c_1 (d_n)^{-1} \max_{1 \leq k \leq p} \left\| \Phi_k^{(\cdot, j_0)} \right\|_2, \quad (49)$$

and

$$\left\| (\Gamma_{j_0}^q(0) - A) \left(\widehat{\Phi}^{(\cdot, j+1)} \right) \right\|_{\infty} \leq c_2 \left\| \widehat{\Phi}^{(\cdot, j+1)} \right\|_1, \quad (50)$$

for some positive constants c_1, c_2 . Combining equations (48), (49) and (50), and use lemma (3) again for the second term on the right hand side of equation (46), we have:

$$c_1 \max_{1 \leq k \leq p} \left\| \Phi_k^{(\cdot, j_0)} \right\|_2 - c_2 d_n \left\| \widehat{\Phi}^{(\cdot, j+1)} \right\|_1 \leq \frac{d_n n \lambda_n}{(t_{j_0} - t_{j_0-1} \vee \widehat{t}_j)} + k_1 d_n \sqrt{\frac{\log p}{n\gamma_n}}. \quad (51)$$

The right hand side goes to zero based on A2 and A3. Similarly, we can use equation (47) to show that

$$c_1 \max_{1 \leq k \leq p} \left\| \Phi_k^{(\cdot, j_0+1)} \right\|_2 - c_2 d_n \left\| \widehat{\Phi}^{(\cdot, j+1)} \right\|_1 \leq \frac{d_n n \lambda_n}{(t_{j_0+1} - t_{j_0} \vee \widehat{t}_j)} + k_1 d_n \sqrt{\frac{\log p}{n\gamma_n}}. \quad (52)$$

Putting the last two equations together implies that:

$$\max_{1 \leq k \leq p} \left| \left\| \Phi_k^{(\cdot, j_0+1)} \right\|_2 - \left\| \Phi_k^{(\cdot, j_0)} \right\|_2 \right| = o(1), \quad (53)$$

which contradicts with Assumption A3. This completes the proof. \square

Proof of Theorem 3. The proof is similar to the proof of Theorem 2.3 in Chan *et al.* (2014). Here we will mention the proof of the first part. For that, assume $|\mathcal{A}_n| < m_0$. This means there exist an isolated true break point, say t_{j_0} . More specifically, there exists an estimated break point \widehat{t}_j such that, $t_{j_0} - t_{j_0-1} \vee \widehat{t}_j \geq n\gamma_n/3$ and $t_{j_0+1} \wedge \widehat{t}_{j+1} \geq n\gamma_n/3$. Applying Lemma 2 twice, we get:

$$\left\| \sum_{l=t_{j_0-1} \vee \widehat{t}_j}^{t_{j_0}-1} Y_{l-1} Y'_{l-1} \left(\Phi^{(\cdot, j_0)} - \widehat{\Phi}^{(\cdot, j+1)} \right) \right\|_{\infty, \mathcal{I}} \leq n\lambda_n + \left\| \sum_{l=t_{j_0-1} \vee \widehat{t}_j}^{t_{j_0}-1} Y_{l-1} \varepsilon'_l \right\|_{\infty} \quad (54)$$

and

$$\left\| \sum_{l=t_{j_0}}^{t_{j_0+1} \wedge \hat{t}_{j+1}-1} Y_{l-1} Y'_{l-1} \left(\Phi^{(\cdot, j_0+1)} - \widehat{\Phi}^{(\cdot, j+1)} \right) \right\|_{\infty, \mathcal{I}} \leq n\lambda_n + \left\| \sum_{l=t_{j_0}}^{t_{j_0+1} \wedge \hat{t}_{j+1}-1} Y_{l-1} \varepsilon'_l \right\|_{\infty}. \quad (55)$$

Now, similar argument as in Theorem 2 reaches to contradiction, and this completes the proof. \square

Proof of Theorem 4. Let's focus on the first part. We show that (a) $\mathbb{P}(\tilde{m} < m_0) \rightarrow 0$, and (b) $\mathbb{P}(\tilde{m} > m_0) \rightarrow 0$. For the first claim, from Theorem 3, we know that there are points $\hat{t}_j \in \mathcal{A}_n$ such that $\max_{1 \leq j \leq m_0} |\hat{t}_j - t_j| \leq n\gamma_n$. By similar arguments as in Lemma 4, we get that there exists a constant $K > 0$ such that:

$$L(\hat{t}_1, \dots, \hat{t}_{m_0}; \eta_n) \leq \sum_{t=q}^T \|\varepsilon_t\|_2^2 + Km_0 n\gamma_n d_n^{*2}. \quad (56)$$

To see this, we only show the calculations for one of the estimated segments. Suppose $s_{i-1} < t_j < s_i$ with $|t_j - s_{i-1}| \leq n\gamma_n$. Denote the estimated coefficient in the segment (s_{i-1}, s_i) by $\hat{\theta}$. Similar to case (b) in the proof of lemma 4, we have:

$$\begin{aligned} \sum_{t=t_j}^{s_i-1} \|y_t - \hat{\theta} Y_{t-1}\|_2^2 &\leq \sum_{t=t_j}^{s_i-1} \|\varepsilon_t\|_2^2 + c_3 |s_i - t_j| \|\Phi^{(\cdot, j+1)} - \hat{\theta}\|_2^2 + c' \sqrt{|s_i - t_j| \log p} \|\Phi^{(\cdot, j+1)} - \hat{\theta}\|_1 \\ &\equiv \sum_{t=t_j}^{s_i-1} \|\varepsilon_t\|_2^2 + I + II. \end{aligned} \quad (57)$$

Now, by the convergence rate of the error (see, e.g., case (b) in the proof of Lemma 4) we can bound both terms I and II:

$$\begin{aligned} I &\leq 4c_3 |s_i - t_j| d_n^* \left(c \sqrt{\frac{\log p}{|s_i - t_j|}} + M_{\Phi} d_n^* \frac{n\gamma_n}{|s_i - t_j|} \right)^2 \\ &= O_p \left(n\gamma_n d_n^{*2} \right), \end{aligned} \quad (58)$$

$$\begin{aligned} II &\leq c' \sqrt{|s_i - t_j| \log p} d_n^* \left(c \sqrt{\frac{\log p}{|s_i - t_j|}} + M_{\Phi} d_n^* \frac{n\gamma_n}{|s_i - t_j|} \right) \\ &= O_p \left(n\gamma_n d_n^{*2} \right). \end{aligned} \quad (59)$$

Moreover, a similar argument needs to be applied to the smaller segment (s_{i-1}, t_j) :

$$\begin{aligned} \sum_{t=s_{i-1}}^{t_j-1} \|y_t - \hat{\theta} Y_{t-1}\|_2^2 &\leq \sum_{t=s_{i-1}}^{t_j-1} \|\varepsilon_t\|_2^2 + c_3 |t_j - s_{i-1}| \|\Phi^{(\cdot, j)} - \hat{\theta}\|_2^2 + c' \sqrt{|t_j - s_{i-1}| \log p} \|\Phi^{(\cdot, j)} - \hat{\theta}\|_1 \\ &\leq \sum_{t=s_{i-1}}^{t_j-1} \|\varepsilon_t\|_2^2 + 2c_3 |t_j - s_{i-1}| \left(\|\Phi^{(\cdot, j+1)} - \hat{\theta}\|_2^2 + \|\Phi^{(\cdot, j+1)} - \Phi^{(\cdot, j)}\|_2^2 \right) \\ &\quad + c' \sqrt{|t_j - s_{i-1}| \log p} \left(\|\Phi^{(\cdot, j+1)} - \hat{\theta}\|_1 + \|\Phi^{(\cdot, j+1)} - \Phi^{(\cdot, j)}\|_1 \right) \\ &= \sum_{t=s_{i-1}}^{t_j-1} \|\varepsilon_t\|_2^2 + O_p \left(n\gamma_n d_n^{*2} \right). \end{aligned} \quad (60)$$

Finally,

$$\begin{aligned} \eta_{(s_{i-1}, s_i)} \|\hat{\theta}\|_1 &\leq \eta_{(s_{i-1}, s_i)} \left(\|\Phi^{(\cdot, j+1)} - \hat{\theta}\|_1 + \|\Phi^{(\cdot, j+1)}\|_1 \right) \\ &= O_p(d_n^*). \end{aligned} \quad (61)$$

Putting them all together leads to:

$$\sum_{t=s_{i-1}}^{s_i-1} \|y_t - \widehat{\theta}Y_{t-1}\|_2^2 + \eta_{(s_{i-1}, s_i)} \|\widehat{\theta}\|_1 = \sum_{t=s_{i-1}}^{s_i-1} \|\varepsilon_t\|_2^2 + O_p\left(n\gamma_n d_n^{*2}\right). \quad (62)$$

Adding them all over all the $m_0 + 1$ segments yields to equation 56.

Now, applying Lemma 4, we get:

$$\begin{aligned} IC(\tilde{t}_1, \dots, \tilde{t}_{\tilde{m}}) &= L_n(\tilde{t}_1, \dots, \tilde{t}_{\tilde{m}}; \eta_n) + \tilde{m}\omega_n \\ &> \sum_{t=q}^T \|\varepsilon_t\|_2^2 + c_1\Delta_n - c_2\tilde{m}n\gamma_n d_n^{*2} + \tilde{m}\omega_n \\ &\geq L(\widehat{t}_1, \dots, \widehat{t}_{m_0}; \eta_n) + m_0\omega_n + c_1\Delta_n - c_2m_0n\gamma_n d_n^{*2} - (m_0 - \tilde{m})\omega_n \\ &\geq L(\widehat{t}_1, \dots, \widehat{t}_{m_0}; \eta_n) + m_0\omega_n, \end{aligned} \quad (63)$$

since $\lim_{n \rightarrow \infty} n\gamma_n d_n^{*2}/\omega_n \leq 1$, and $\lim_{n \rightarrow \infty} m_0\omega_n/\Delta_n = 0$. This proves part (a). To prove part (b), note that a similar argument as in Lemma 4 shows that

$$L_n(\tilde{t}_1, \dots, \tilde{t}_{\tilde{m}}; \eta_n) \geq \sum_{t=q}^T \|\varepsilon_t\|_2^2 - c_2\tilde{m}n\gamma_n d_n^{*2}. \quad (64)$$

A comparison between $IC(\tilde{t}_1, \dots, \tilde{t}_{\tilde{m}})$ and $IC(\widehat{t}_1, \dots, \widehat{t}_{m_0})$ yields to:

$$\begin{aligned} \sum_{t=q}^T \|\varepsilon_t\|_2^2 - c_2\tilde{m}n\gamma_n d_n^{*2} + m\omega_n &\leq IC(\tilde{t}_1, \dots, \tilde{t}_{\tilde{m}}) \\ &\leq IC(\widehat{t}_1, \dots, \widehat{t}_{m_0}) \\ &\leq \sum_{t=q}^T \|\varepsilon_t\|_2^2 + Km_0n\gamma_n d_n^{*2} + m_0\omega_n, \end{aligned} \quad (65)$$

which means:

$$(\tilde{m} - m_0)\omega_n \leq c_2\tilde{m}n\gamma_n d_n^{*2} + Km_0n\gamma_n d_n^{*2}, \quad (66)$$

which contradicts with the fact that $m_0n\gamma_n d_n^{*2}/\omega_n \rightarrow 0$. This completes the first part of the theorem.

For the second part, put $B = 2K/c$. Now, suppose that there exists a point t_i such that $\min_{1 \leq j \leq m_0} |\tilde{t}_j - t_j| \geq Bm_0n\gamma_n d_n^{*2}$. Then, by similar argument as in Lemma 4, we can show that:

$$\begin{aligned} \sum_{t=d}^T \|\varepsilon_t\|_2^2 + cBm_0n\gamma_n d_n^{*2} &< L_n(\tilde{t}_1, \dots, \tilde{t}_{m_0}) \\ &\leq L_n(\widehat{t}_1, \dots, \widehat{t}_{m_0}) \\ &\leq \sum_{t=q}^T \|\varepsilon_t\|_2^2 + Km_0n\gamma_n d_n^{*2}, \end{aligned} \quad (67)$$

which contradicts with the way B was selected. This completes the proof of the theorem. \square

Proof of Theorem 5. Proof of this theorem is similar to Proposition 4.1 in Basu & Michailidis (2015). The two main components of the proof is (i) verifying the restricted eigenvalue (RE) for $\widehat{\Gamma} = I_p \otimes (\mathcal{X}'_r \mathcal{X}_r / N)$, and (ii) verifying the deviation bound for $\left\| \widehat{\gamma} - \widehat{\Gamma} \Phi \right\|_\infty$ where $\widehat{\gamma} = (I_p \otimes \mathcal{X}'_r) \mathbf{Y}_r / N$. Once these two are verified, the rest of the proof is applying deterministic arguments used in Proposition 4.1 in Basu & Michailidis (2015). Therefore, here we proof (i) and (ii) only.

Condition (i) means that there exist $\alpha, \tau > 0$ such that for any $\theta \in \mathbb{R}^{\bar{\pi}}$, we have

$$\theta' \widehat{\Gamma} \theta \geq \alpha \|\theta\|_2^2 - \tau \|\theta\|_1^2,$$

with probability at least $1 - c_1 \exp(-c_2 N)$ for large enough constants $c_1, c_2 > 0$. Based on Lemma B.1 in Basu & Michailidis (2015), it is enough to show the RE for $S = \mathcal{X}'_i \mathcal{X}_i / N$, where \mathcal{X}_i is the i th block component of \mathcal{X}_r . Applying Proposition 2.4 in Basu & Michailidis (2015), we have for any $v \in \mathbb{R}^{pq}$ with $\|v\|_2 \leq 1$, and any $\eta > 0$:

$$\mathbb{P} \left(\left| v' \left(S - \frac{N_i}{N} \Gamma_i(0) \right) v \right| > c\eta \right) \leq 2 \exp(-c_3 N \min(\eta^2, \eta)).$$

Now, to make the above probability hold uniformly on all the vectors v , we apply the discretization Lemma F2 in Basu & Michailidis (2015) and also Lemma 12 in the supplementary materials of Loh & Wainwright (2012) to get:

$$\left| v' \left(S - \frac{N_i}{N} \Gamma_i(0) \right) v \right| \leq \alpha \|v\|_2^2 + \alpha/k \|v\|_1^2,$$

with high probability at least $1 - c_1 \exp(-c_2 N)$, for all $v \in \mathbb{R}^{pq}$, some $\alpha > 0$ and with an integer $k = \lceil c_4 N / \log(pq) \rceil$ with some $c_4 > 0$. This implies that

$$v' S v \geq v' \frac{N_i}{N} \Gamma_i(0) v - \alpha \|v\|_2^2 - \alpha/k \|v\|_1^2 \geq \alpha \|v\|_2^2 - \alpha/k \|v\|_1^2,$$

since $N_i \geq \Delta_n - 4R_n$, $N = n + q - 1 - 2m_0 R_n$, and assuming $\Delta_n \geq \varepsilon n$ implies that $N_i/N \geq \varepsilon \geq 2\alpha$.

The deviation condition (DC) here means that there exist a large enough constant $C' > 0$ such that

$$\left\| \hat{\gamma} - \hat{\Gamma} \Phi \right\|_\infty \leq C' \sqrt{\frac{\tilde{\pi}}{N}},$$

with probability at least $1 - c_1 \exp(-c_2 \log \tilde{q})$. To verify this condition here, observe that $\hat{\gamma} - \hat{\Gamma} \Phi = \text{vec}(\mathcal{X}'_r E_r) / N$. Therefore, denoting the h -th column block of \mathcal{X}_r by $\mathcal{X}_{r,(h)}$, for $h = 1, \dots, (m_0 + 1)q$, we have:

$$\left\| \hat{\gamma} - \hat{\Gamma} \Phi \right\|_\infty = \max_{1 \leq k, l \leq p; 1 \leq h \leq (m_0 + 1)q} \left| e'_k \mathcal{X}'_{r,(h)} E_r e_l \right|.$$

Now, for a fixed k, l, h , applying Proposition 2.4(b) in Basu & Michailidis (2015) gives:

$$\mathbb{P} \left(\left| e'_k \mathcal{X}'_{r,(h)} E_r e_l \right| > k_1 \eta \right) \leq 6 \exp(-k_2 N \min(\eta^2, \eta)),$$

for large enough $k_1, k_2 > 0$, and any $\eta > 0$. Now, setting $\eta = C' \sqrt{\frac{\tilde{\pi}}{N}}$, and taking the union over all the $\tilde{\pi}$ cases for k, l, h yield the desired result. This completes the proof of this theorem. \square